Geometry and compartmentalization of fluvial meander-belt reservoirs at the bar-form scale: quantitative insight from outcrop, modern and subsurface analogues

Luca Colombera*, Nigel P. Mountney, Catherine E. Russell, Michelle N. Shiers, William D. McCaffrey

Fluvial & Eolian Research Group, School of Earth & Environment, University of Leeds, Leeds, LS2 9JT, UK

*) corresponding author. E-mail: l.colombera@leeds.ac.uk

Abstract

The preserved deposits of fluvial meander belts typically take the form of patchworks of sand-prone bar-form elements bordered by genetically related, muddy channel fills. In meander belts that act as hydrocarbon reservoirs, characteristics of sedimentary architecture, including the geometry of point-bar elements and the internal compartmentalization exerted by the presence of mud-prone abandoned channel fills, control the effectiveness of primary and enhanced hydrocarbon recovery. Therefore, a quantitative description of meander-belt architectures is desired to provide constraints to subsurface predictions.

To this end, an examination of sedimentological datasets, enabled by database-assisted analysis, is undertaken. Sixty-four database case studies of modern, ancient outcropping and subsurface fluvial depositional systems are characterized in a quantitative manner, to assess the relative importance of different styles of lithological compartmentalization, and to provide constraints that can be applied to inform predictions of the geometry and connectivity of bar-scale sandbodies in meander-belt reservoirs. The results of this study include: (i) a set of empirical relationships that relate dimensional parameters describing the geometry of point-bar elements, associated channel fills, channel complexes and potentially unswept compartments; (ii) probabilistic descriptions that relate well density to both the proportion of compartments intersected by a well array, and the maximum volume of untapped bar-form compartments.

The resulting predictive tools can be applied to assist reservoir development and production, either directly or through incorporation into reservoir models. For example, it is shown how to use these quantitative constraints to predict the likely volume of point-bar reservoir compartments with potential bypassed hydrocarbons, and to optimize drilling strategies (e.g., whether and how to perform infill drilling or horizontal drilling), by providing a measure of the likely presence, size, spacing, and orientation of bypassed hydrocarbon volumes.

Keywords: point bar; abandoned channel; meandering; sandstone; connectivity; fluvial reservoir; reservoir compartment; fluvial aquifer.

1. Introduction

1.1 Bar-scale meander-belt compartmentalization

Channel belts deposited by meandering rivers commonly form hydrocarbon reservoirs or fluvial aquifers that consist of mosaics of sand-prone bar-form and channel-fill elements. Muddy and organic-rich deposits dominate the infill of abandoned channels that have been isolated from river flow by processes of meander cut-off or meander-belt avulsion, becoming sites at which low-energy deposition prevails (cf. Fisk 1947; Guccione et al. 1999; Toonen et al. 2012; and references therein). Where these mud-prone abandoned channel fills border genetically related sand-rich macroforms, they may act as barriers or baffles to hydrocarbon flow, and, as a result, they can compartmentalize meander-belt reservoirs (Figure 1). The potential importance of the compartmentalization of meander-belt reservoir by mud-prone abandoned channel fills, and its important control on sand connectivity and effectiveness of primary and secondary hydrocarbon recovery, are widely recognized (Berg 1968; Busch 1974; Richardson et al. 1987; Ambrose et al. 1991; Jordan & Pryor 1992; Galloway & Hobday 1996; Weimer et al. 1998; de Rooij et al. 2002; Edie & Andrichuk 2003; Jiao et al. 2005; Donselaar & Overeem 2008; Shepherd 2009; Reijenstein et al. 2011; Alpak & Barton 2014; Shu et al. 2015; and references therein). Yet, this problem is typically described and considered at a qualitative level. This is significant, given that a number of oil and gas reservoirs are hosted in fluvial meander belts in which the style of compartmentalization described above is documented to have influenced production. Examples of reservoirs subject to point-bar compartmentalization by channel fills include those of the Little Creek field (Mississippi, USA; Werren et al. 1990), the Elmwood field (Oklahoma, USA; Cornish 1984), the Widuri field (Java Sea; Carter 2003), the Campbell-Namao field (Alberta, Canada; Edie & Andrichuk 2005), the Sorrento field (Colorado, USA; Sonnenberg 1990), the Gudao field (China; Wu et al. 2008), the Peoria field (Colorado, USA; Chapin & Meyer 1991), the Seeligson and Stratton fields (Texas, USA; Ambrose et al. 2008), the Platong field (Gulf of Thailand; Pakdeesirote et al. 2016), and gas fields in the Quaternary of the Gulf of Thailand (e.g., de Rooij et al. 2002). Given the frequency with which this style of stratigraphic compartmentalization is observed, and how it is seen to affect hydrocarbon production, the recognition of meander-belt architectures in subsurface datasets should forewarn of the likely influence of intra-channel-belt compartmentalization. Because it is advocated that the evaluation of styles of compartmentalization should be undertaken in the early appraisal stages of the exploration and production workflow (Smalley & Hale 1996; Fox & Bowman 2010; Jolley et al. 2010; Smalley & Muggeridge 2010), there is a need for predictive tools that can be used in this context.

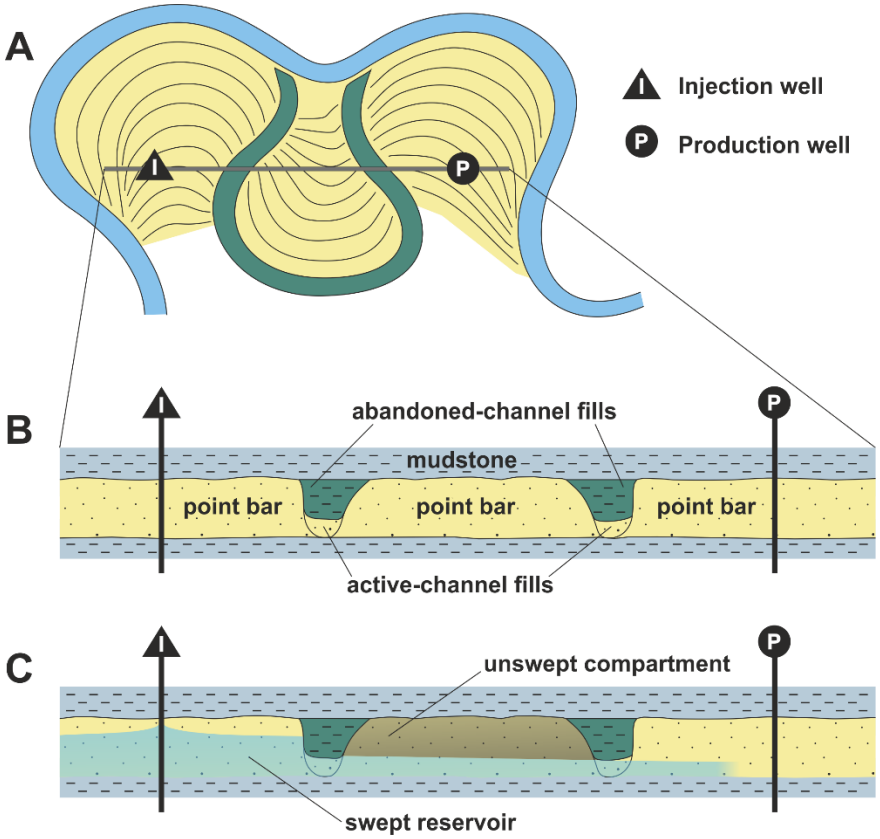

Figure 1. (A) Planform view of an idealized meander belt made of sandy point bars and mud-prone abandoned-channel-fill deposits. **(B)** Cross-section of the idealized preserved sedimentary architecture of a meander belt of the type represented in part A, representing deposits consisting of point-bar sands, active and passive channel fills, and overbank and/or marine mudstones. **(C)** Representation of the compartmentalization of the upper part of point bars determined by muddy abandonment deposits, with reference to the architecture represented in parts A and B and to the particular arrangement of injection and production wells represented; it is shown how the development of attic reservoir compartments might result in poor sweep efficiency in a scenario of oil production by waterflooding.

1.2 Aim, objectives and outline

The scope of this work is to provide quantitative insight into meander-belt compartmentalization by leveraging information from many geological analogues, in particular by examining outcrop, modern, and subsurface examples of fluvial depositional systems that display bar-form and channel-form architectures analogous to those described above. The aims are to assess the likelihood of different styles of compartmentalization, and to synthesize quantitative information that can be applied to inform development and production of meander-belt reservoirs, either directly or through its incorporation in reservoir models. In particular, a set of predictive relationships are compiled based on the characterization of these analogues, and which find application to:

- predict the likely volume of bars that might represent stratigraphic traps, and of reservoir compartments with potential unswept oil;

- guide optimal well placement, by providing a measure of the likely size and spacing of bars;

- optimize production strategies (e.g., whether or not to operate infill drilling or horizontal drilling, choice of well spacing), by providing a measure of the likely presence and size of bypassed volumes.

A quantitative description of point-bar geometries and connectivity might also find applications in contexts of: (i) point-bar aquifer contamination and clean-up, (ii) geothermal energy exploitation from hot sedimentary aquifers (HSA's) of fluvial origin, and (iii) carbon-dioxide capture and storage.

After introducing the database employed in this research, an analysis of bar geometries is presented, and its implications for reservoir production discussed. This is followed by an assessment of styles of meander-belt compartmentalization by mud plugs, and by a quantification of compartment volumes. Then, further empirical analysis is presented that provides geometrical constraints for informing optimal well placement in meander-belt reservoirs, partly on a probabilistic basis.

2. Materials and methods

Results presented in this work describe the geometry and connectivity of meander belts at the bar-form and channel-form scale, based on the analysis of multiple geological analogues. Results arise from a compound analysis of case studies contained in a database of sedimentary architecture, the Fluvial Architecture Knowledge Transfer System (FAKTS; Colombera et al. 2012; 2013). FAKTS contains data on sedimentary units belonging to multiple scales of observation, assigned to depositional systems that are classified on a number of attributes describing their depositional context and boundary conditions. FAKTS includes data on the geometry and spatial relationships of the sedimentary bodies. Datasets are in large part coded from the published scientific literature, but unpublished data collected by the authors of the current work are also included. The database can be filtered on depositional-system types, sedimentological properties, or metadata, in order to return relevant information in quantified form.

This study makes use of data from both modern rivers and ancient successions of interpreted fluvial origin. Most of the data considered are derived from channel belts associated with – or interpreted to have been deposited by – meandering rivers; additional data related to generic lateral-accretion bars recognized in the stratigraphic record but not classified in terms of channel pattern are included. An account of all the case studies and data sources is provided in Table 1. Overall, the information presented derives from a quantitative characterization of 1259 architectural elements (1139 bars, 120 channel fills), from 64 case studies stored in FAKTS. Five-hundred-and-seventy-four bars represent modern geomorphological elements.

Morphometric parameters that describe the cross-sectional and planform morphology of point bars derived from outcrop studies conducted on cross-section and planform exposures are complemented with descriptions of point-bar planform morphology obtained from studies of the geomorphological organization of modern rivers, based on interpretation of satellite and aerial photographs, and from interpreted seismic time slices. Any inference made from

rock-record examples is subject to the fundamental uncertainty related to the interpretation of facies associations and architectural properties in terms of sub-environment of deposition.

Statistical analyses of the morphometric parameters of bars and channel fills have been undertaken through (i) calculation of descriptive statistics, (ii) regression, to model their relationships, and (iii) statistical tests, to determine types of distributions in families of bars. Building on these analyses, probabilistic models based on principles of geometric probability (Sinclair 1975; Shurygin 1976) are introduced that can be employed to predict the proportion of bars and the size of reservoir compartments that may contain bypassed hydrocarbons, from knowledge of borehole spacing and thickness of point-bar deposits.

Table 1. Case studies stored in the FAKTS database that have been queried to derive analogue information on laterally accreting barforms or point bars. The table reports references to published data sources, the number of studied bars, and the stratigraphic unit or modern river subject of each study. Datasets employed in the formulation of empirical relationships are indicated. (Fm. = Formation; Mb. = Member; Gp. = Group). Case-study Identification Numbers (ID) relate to those coded in the FAKTS database. N = number of bar-form elements considered for each case study.

ID	Reference	N	Stratigraphic unit or modern river	In empirical relationships?
1	Miall (1988)	3	Kayenta Fm.	
2	Hornung & Aigner (1999)	20	Middle-Upper Stubensandstein	Yes
5	Carter (2003)	5	Talang Akar Fm.	Yes
9	Jones et al. (2001)	4	Rio Vero Fm.	Yes
17	Jordan & Pryor (1992)	4	Mississippi	Yes
20	Jo (2003)	3	Sindong Gp.	Yes
21	Cuevas Gozalo & Martinius (1993)	46	Upper Unit, Tortola fluvial system	Yes
23	Cain (2009)	3	Organ Rock Fm.	Yes
25	Stephens (1994)	7	Kayenta Fm.	Yes
26	*original study*	22	Kayenta Fm.	Yes
29	Fabuel-Perez et al. (2009a)	2	Oukaimeden Fm.	
31	Fabuel-Perez et al. (2009b)	2	Oukaimeden Fm.	
33	Fielding et al. (1993)	10	Rangal Coal Measures	
41	Santos et al. (2014)	10	Guarda Velha Fm.	
44	Pranter et al. (2007)	2	Lower Williams Fork Fm.	
45	Donselaar & Overeem (2008)	16	Sariñena Fm.	Yes
46	Corbeanu et al. (2004)	2	Ferron Sandstone Mb., Mancos Shale	Yes
51	Labourdette (2011)	1	Olson Mb., Escanilla Fm.	Yes
58	Olsen (1989)	2	Dinosaur Canyon Mb., Moenave Fm.	Yes
59	Catuneanu & Elango (2001)	5	Balfour Fm., Beaufort Gp.	
60	Catuneanu & Bowker (2001)	1	Middleton Fm. and Koonap Fm., Beaufort Gp.	
61	Miall & Turner-Peterson (1989)	11	Morrison Fm.	Yes
69	Olsen (1995a)	2	Price River Fm. and North Horn Fm.	Yes
71	Opluštil et al. (2005)	4	Kladno Fm. and Týnec Fm.	Yes
73	Stewart (1983)	11	Wessex Fm., Wealden Gp.	Yes
74	Stewart (1983)	11	Fairlight Clay and Ashdown Beds Fm., Hastings Beds Gp.	Yes
77	Ori (1982)	11	Reno	Yes

78	Martinius & Nieuwenhuijs (1995)	49	Upper Unit, Tortola fluvial system	Yes
80	Rygel & Gibling (2006)	8	Joggins Fm.	Yes
84	Ori & Penney (1982)	8	Templetown Fm. and Harrylock Fm., Old Red Sandstone	Yes
88	Olsen (1987)	3	Upper Bunter Sand, Bunter Sandstone Fm., Bacton Gp.	
100	Viseras et al. (2006)	1	Late Pliocene, Guadix Basin	Yes
102	Sánchez-Moya et al. (1996)	2	Buntsandstein	Yes
103	Limarino et al. (2001)	2	Vinchina Fm.	
104	Ferguson & Brierley (1999)	3	Tuross	Yes
106	Mack et al. (2003)	5	Abo Fm.	
109	Roberts (2007)	12	Kaiparowits Fm.	
111	Kraus & Middleton (1987)	1	Glenns Ferry Fm.	
116	Jablonski (2012)	4	McMurray Fm.	
117	Hirst (1991)	18	Sariñena Fm.	Yes
121	Trendell et al. (2013)	14	Chinle Fm.	
136	Olsen (1995b)	12	North Horn Fm.	
139	Rasmussen (2005)	17	Colton Fm.	Yes
144	Ford & Pyles (2014)	2	Middle Wasatch Fm.	Yes
147	Sendziak (2012)	15	Lower Wasatch Fm.	Yes
153	Ghinassi et al. (2013)	2	Goreya Fm.	Yes
154	Keighley et al. (2003)	4	Middle Green River Fm.	
156	Kerr et al. (1999)	1	Bartlesville Sandstone Mb., Boggy Fm.	
158	Ielpi & Ghinassi (2014)	34	Scalby Fm.	Yes
159	Blum et al. (2013)	86	Composite database	Yes
160	Bridge et al. (1995)	1	South Esk	Yes
164	Hubbard et al. (2011)	12	McMurray Fm.	Yes
166	*original study*	21	Neslen Fm., Mesaverde Gp.	
170	Fachmi & Wood (2005)	25	Arang Fm. and Muda Fm.	Yes
171	Maynard & Murray (2003)	14	Arang Fm.	Yes
173	Maynard et al. (2010)	10	Grand Rapids Fm.	Yes
175	Miall (2002)	5	Pilong Fm.	Yes
176	Boeser (2011)	56	Ganges	Yes
177	Feng (2000)	114	Late Quaternary Gulf of Thailand	Yes
178	Schenk (1992)	69	Composite database	Yes
179	Anderson (2005)	5	Iles Fm., Mesaverde Gp.	Yes
180	Smith (1987)	6	Teekloof Fm., Beaufort Gp.	Yes
182	Reijenstein et al. (2011)	63	Late Quaternary Gulf of Thailand	Yes
-	*original study*	215	Composite database	Yes

3. Analysis of bar-form geometries

The geometry of point bars or laterally accreting macroforms is described by values of maximum thickness, cross-stream width, and down-stream length. Apparent widths are recorded along a direction at an angle with true cross-stream direction, or at a position offset from the one of maximum width (Figure 2A). Width measures are classified as 'partial' or 'unlimited', *sensu* Geehan & Underwood (1993), whenever the position of lateral pinch-out of the bar-form bodies is unknown (e.g., not exposed due to outcrop termination), at one or

both ends, respectively (Figure 2A). Data on apparent, partial and unlimited measures, which will typically underestimate true dimensions (Figure 2B), have been excluded from most subsequent analyses presented later in this paper.

Data have been employed to compile empirical relationships for predictions of bar-form width and length from their thickness, on the basis of which geometrical models that describe point-bar volumes are derived. The domain of bar thickness may exceed the range covered by the data in Figure 2; for example, exceptionally thick bars of the Cretaceous McMurray Formation (Alberta, Canada) are seen to reach over 65 m in thickness (Blum 2012).

Positive relationships are seen between bar thickness, width, and length, as expected in consideration of known relationships between water discharge, channel hydraulic geometry, meander wavelength, and river migration rates (Leopold & Wolman 1960; Nanson & Hickin 1986). Power-law regression curves have been derived to describe the relationships between bar-form width and thickness (Figure 2C-D), and between length and width (Figure 2C-D), based on regression of data from individual bars.

It is noted that predictions of bar-form widths from known thickness attempted by the equation in Figure 2C are more conservative than those predicted by relationships proposed previously by:

- Blum et al. (2013), as based on a comparable dataset; this is true for most values of thickness, with the exception of very large bars (40+ m in thickness);
- Schenk (1992), based on a combination of relations between formative-channel hydraulic geometry and bar geometries (in part following work by: Leeder 1973; Allen 1984), corrected for sediment compaction following recommendations by Ethridge & Schumm (1978). As acknowledged by Schenk (1992), this discrepancy is in part accounted for by the error in relating channel depth to bar-form thickness, particularly given that the former varies along a channel bend (Jackson 1981; Willis & Tang 2010).

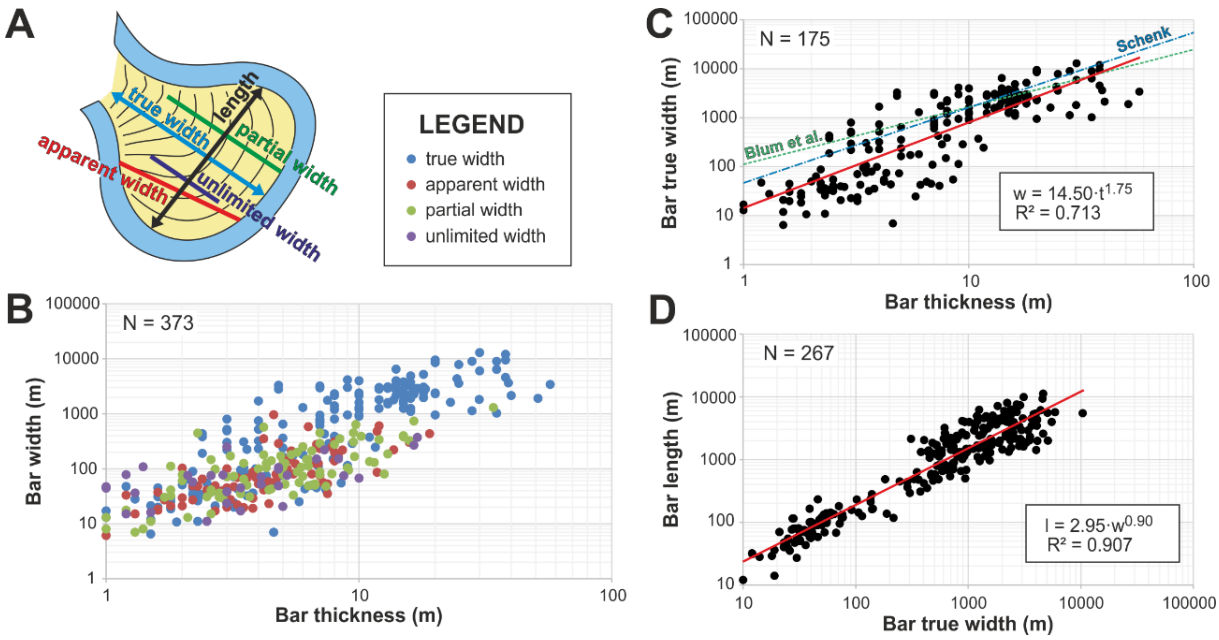

Figure 2. (A) Classification of bar-form cross-stream widths and down-stream lengths by quality of observation, i.e., as true, apparent, partial, or unlimited (see text). **(B)** Cross-plot of width vs. thickness for point bars and laterally accreting barforms, with data points colour-coded by quality of observation, as in legend and part A. **(C)** Cross-plot of width vs. thickness for point bars and laterally accreting barforms that only includes true widths; a power-law empirical equation has been fitted to the data (in red), and compared with corresponding relationships by Schenk (1992) and Blum et al. (2013). **(D)** Cross-plot of length vs. width for point bars and laterally accreting barforms that only includes true widths and lengths; a power-law empirical equation has been fitted to the data. For each pair of variables, empirical relationships are reported in respective boxes, with associated coefficients of determination.

For values of width larger than 10 m, predictions of bar-form length from known width by the equation in Figure 2D are more conservative than those predicted by a corresponding relationship by Holzweber et al. (2014), originally presented in a form for predicting bar width from length and solely based on modern-river data. However, width and length measures provided by Holzweber et al. (2014) are related to the “active” part of a bar only, and thus are likely not comparable with data in the current work. This might also partly reflect the fact that expanding point bars that are now being deposited next to active channels (i.e., are pre-abandonment) are expected to be on average narrower than they will be at the time of meander cut-off (cf. expected relationship between length-to-width ratio and sinuosity; Willis & Tang 2010).

Additionally, a set of power-law regression curves have been derived that express descriptive statistics of bar width and length as functions of mean bar thickness and width, for bars contained in different successions (Figure 3). These descriptive statistics relate to stratigraphic intervals that are established and recorded in FAKTS to capture stratigraphic variations in depositional-system characteristics or boundary conditions (Colombera et al. 2012). In particular, these equations relate (i) mean and standard deviation in bar width to mean bar thickness (Figure 3A-B), (ii) mean and standard deviation in bar length to mean bar width (Figure 3C-D), and (iii) mean and standard deviation in bar length to mean bar

thickness (Figure 3E-F). These equations are applicable to predictions of bar-form size distributions relative to stratigraphic intervals that contain multiple channel belts.

Beside the use made later in this work, the relationships presented in Figures 2 and 3 have general predictive value, even beyond the scope of reservoir development planning. In exploration contexts, data of this type can be considered in relation to the depositional setting of the analysed bars, on which FAKTS case studies are classified, to identify the potential presence of stratigraphic traps that may represent attractive exploration targets. This might be especially relevant to point-bar deposits associated with giant rivers, which may form stratigraphic traps of significant size (cf. Busch 1974; Berg 1981; Leo 1997; Edie & Andrichuk 2003; Fustic et al. 2012). For example, database analysis highlights that many examples from the high-end of the spectrum of bar size (20 to 60 m in thickness; up to 7000 m in width) were deposited in continental-shelf settings, when the shelf was exposed at lowstand (Feng 2000; Posamentier 2001; Miall 2002; Carter 2003; Reijenstein et al. 2011). It is likely that at lowstand the amalgamation of drainage areas, which otherwise form separate catchments during highstand, results in rivers that are on average significantly larger than rivers on continents at highstand (cf. Voris 2000; Miall 2006; Blum & Hattier-Womack 2009). Modern rivers, and associated landforms and deposits, may not represent good analogues to systems of this type, in terms of scale and scale-dependent processes. The analysed data support the view that the development of large rivers over continental shelves might be a recurrent mechanism to the generation of bars of large volume, which may act as stratigraphic traps when sealed by highstand mudstones.

Furthermore, the relationships presented above can be applied for the following purposes:

- To condition stochastic reservoir models for meander belts, in which point-bar elements are modelled as discrete units, and which can be applied to well-placement optimization algorithms (e.g., Cullick et al. 2005; Liu & Jalali 2006; Ding et al. 2014; and references therein); this can be achieved by employing descriptive statistics of bar-form size as direct input to object-based reservoir-modelling algorithms, or to constrain indicator-variogram ranges empirically (Ritzi 2000; cf. Colombera et al. 2016) to permit conditioning of pixel-based simulations;
- To guide horizontal well-to-well correlations of bar-scale sandbodies, either by informing the correlation of individual bars employing the relationships in Figure 2, or by incorporating results presented in Figure 3 into so-called ‘correlability’ models (Colombera et al. 2014), against which the realism of correlation panels can be assessed;
- To inform the density and orientation of horizontal wells, if horizontal drilling is performed to confront intra-channel-belt compartmentalization; Figure 2D suggests that, in cases of channel complexes made of multiple laterally stacked bars, it might be preferable to arrange horizontal wells oriented orthogonally to the channel-belt axis, given that point-bar lengths are commonly larger than widths (length-to-width ratios range from 0.35 to 6.87, with an average of 1.90). This will result in each well having a larger probability of intersecting multiple bars and in a larger proportion of bars intersected per borehole length, thus allowing wider well separation. Nonetheless, it must be acknowledged that opposite recommendations could be made if intra-bar compartmentalization related to facies-scale heterogeneities is recognized, for example due to the presence of mud drapes (cf. Pranter et al. 2007).

On the basis of relationships between morphometric parameters, as given in Figures 2 and 3, the likely volume of individual bars can be estimated from knowledge of one of the dimensional parameters. By combining relationships between bar width and thickness, and between bar length and width (Figure 2), expressions that relate base-case scenarios of likely bar volume as a function of their thickness have been compiled (Figure 4). To treat uncertainty in the three-dimensional shape of the bars, three cases are considered that assume bars with planform shape that is half circular, half elliptic, or crescentic. The bar thickness is assumed constant throughout the sandbody. Formulas for estimating bar volumes from measurements of bar thickness, width and dip length are given in Figure 4A for the three shape types. For a certain value of bar thickness, bars with half circular planform shape will be larger by volume than half-elliptic and crescentic ones, the two of which are approximately equivalent (Figure 4B).

Results in Figure 4B provide estimates of the volume of a bar. The size of a bar-scale reservoir compartment or stratigraphic trap is likely to be also controlled by the geometry of mud plugs that might be juxtaposed laterally to the bars.

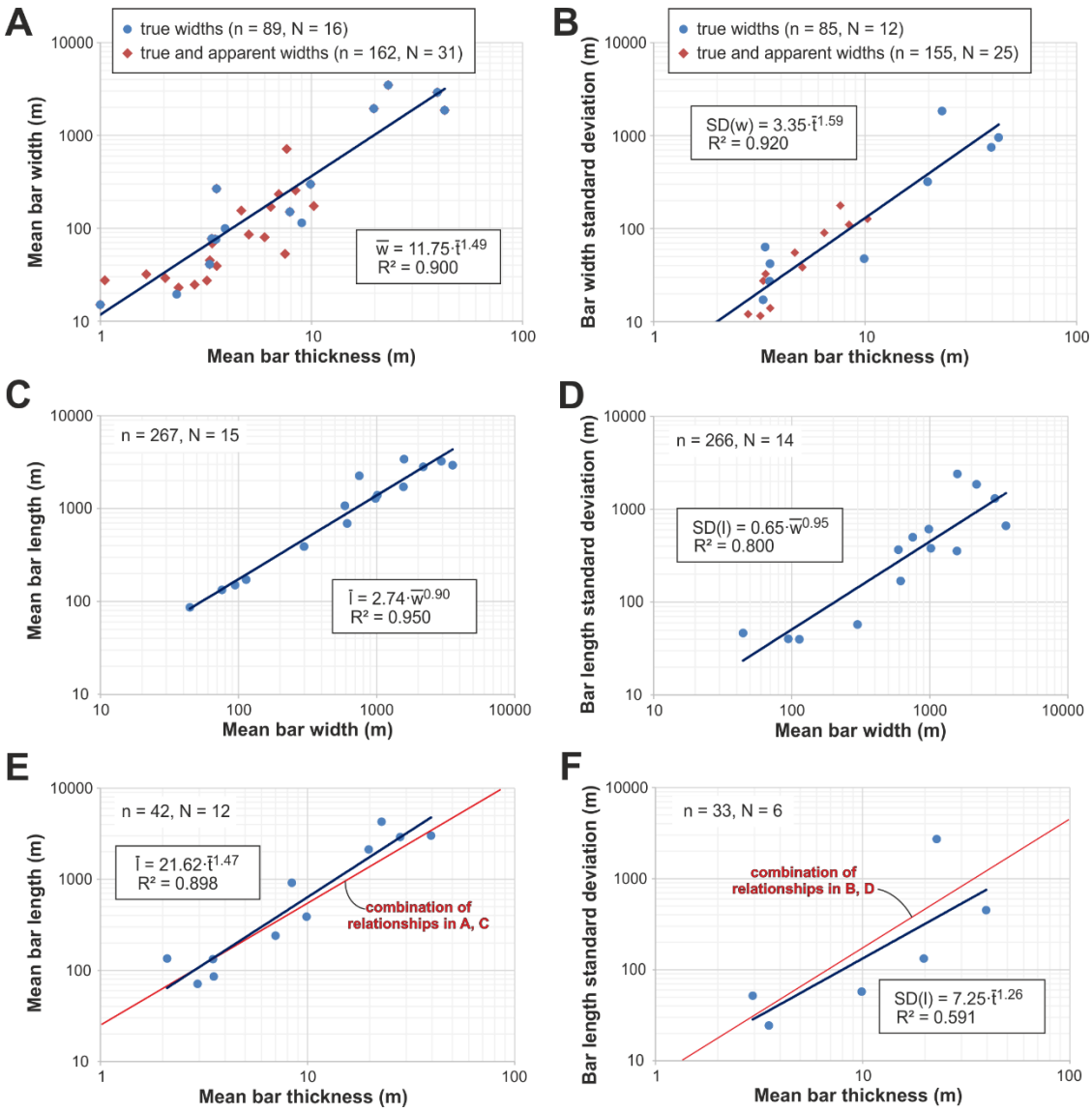

Figure 3. (A) Cross-plot of mean bar width vs. mean bar thickness, as evaluated by stratigraphic interval; blue spots represent data that only include true-width measurements, whereas red squares represent data that also include apparent measurements; a best-fit power-law relationship has been fitted to true-width data. **(B)** Cross-plot of bar width standard deviation vs. mean bar thickness, as evaluated by stratigraphic interval; blue spots represent data that only include true-width measurements, whereas red squares represent data that also include apparent measurements; a best-fit power-law relationship has been fitted to true-width data. **(C)** Cross-plot of mean bar length vs. mean bar width, as evaluated by stratigraphic interval; a best-fit power-law relationship has been fitted to the data. **(D)** Cross-plot of bar length standard deviation vs. mean bar width, as evaluated by stratigraphic interval; a best-fit power-law relationship has been fitted to the data. **(E)** Cross-plot of mean bar length vs. mean bar thickness, as evaluated by stratigraphic interval; a best-fit power-law relationship has been fitted to the data; a corresponding prediction based on combination of relationships in A and C is also shown (in red). **(F)** Cross-plot of bar length standard deviation vs. mean bar thickness, as evaluated by stratigraphic interval; a best-fit power-law relationship has been fitted to the data; a corresponding prediction based on combination of relationships in A and D is also shown (in red). For each pair of variables, empirical relationships are reported in respective boxes, with associated coefficients of determination. 'N' denotes the number of stratigraphic intervals considered; 'n' denotes the number of bars considered.

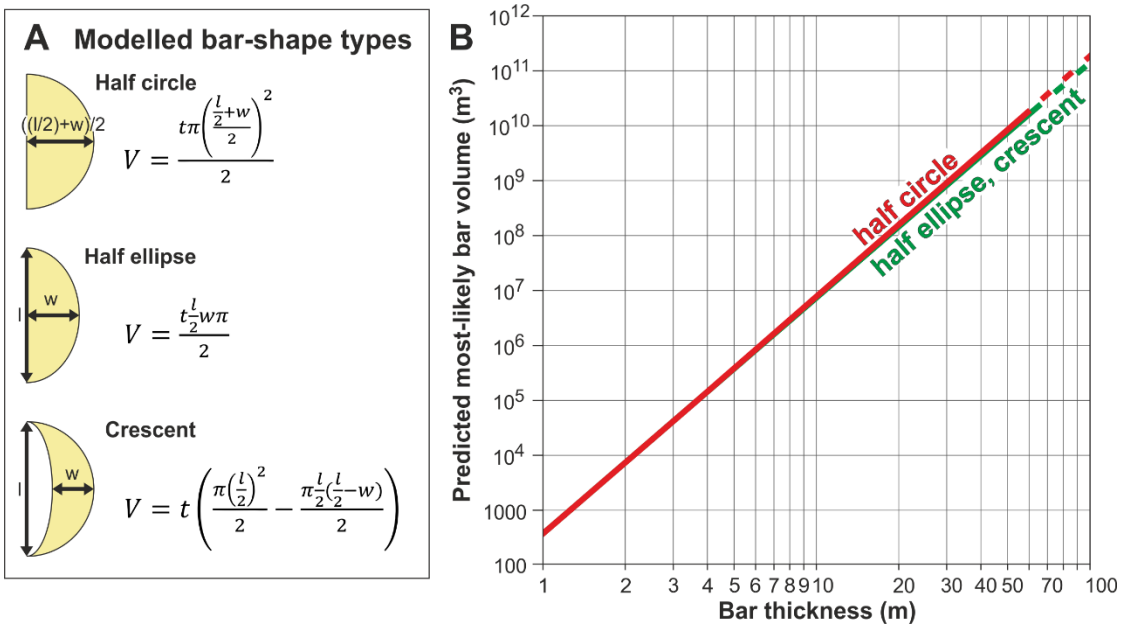

Figure 4. (A) Types of planform shapes considered for estimations of base-case point-bar volumes: half circle, half ellipse, and crescent; the reported formulas for bar volume in each of the three cases assume constant bar thickness (t), and the represented relationships between measures of bar width (w) and length (l) and the morphometric parameters of the three shape types. **(B)** Base-case estimates of bar volumes for the three scenarios of shape types represented in A, expressed as functions of bar thickness, based on the application of empirical relationships relating bar thickness, width, and length (Figure 2C-D). Note logarithmic scales. Volume estimates for bars with crescent or half-elliptical planform shapes are not discernible in figure at the chosen scale, and are therefore represented with the same curve.

4. Analysis of meander-belt compartmentalization

4.1 Assessment of compartmentalization style

In fluvial successions deposited by meandering rivers, channel-belt deposits can be conceptualized as being made of point bars that are either (i) entirely compartmentalized by mud plugs, representing the infill of abandoned channels, or (ii) connected through base-of-channel thalweg sands or gravels, in a so-called string-of-beads fashion (Donselaar & Overeem 2008). Thus, fluvial successions with string-of-beads architecture will display higher static connectivity, for a given value of net-to-gross ratio (Donselaar & Overeem 2008).These are just idealized end-member scenarios: in reality it is plausible that channel belts might display both behaviours, i.e., may contain bars that are isolated, and bars that are connected to others by base-of-channel reservoir-quality deposits. FAKTS data are used to test the relative prevalence of these two end-member models of meander-belt architecture. In particular, database output is used to quantify the degree to which the chosen geological analogues approximate each of the models. This is achieved in two ways, by quantifying (i) the relative thickness of bars and laterally transitional abandoned channel fills (Figure 5A-B), and (ii) the average thickness of bars and mud plugs in stratigraphic intervals (Figure 5C).

All the information on the thickness of bars and channel fills (Figure 5A-C) is effectively based on “snapshots” of the architecture of meander-belt deposits at some locations. Sand-prone deposits recording active-channel deposition, including those accumulated in the bar-form body as well as base-of-channel sands, are seen to display variable thickness along a sinuous reach. For example, sands are expected to reach a maximum thickness at the apex of a meander, where scour pools occur (Krinitzsky 1965; Keller & Melhorn 1978; Jackson 1981; Smith 1987; Willis & Tang 2010). Additionally, variability in the thickness of sand accumulated in the channel thalweg might relate to the relative rates of bar migration and thalweg aggradation in response to levee build up (cf. van Toorenenburg et al. 2016).

When considering information on the relative size of adjacent bars and channel fills (Figure 5A-B), it must be noted that a mud plug can be thicker than a laterally adjacent bar (and thus the thickness ratio can be larger than unity; Figure 5A). A reason for this is that the data describe spatial – and not necessarily genetic – relationships. In other words, for each value of relative thickness, the channel fill may not record the channel that is genetically related to the bar itself, but may rather represent the product of infill of a deeper channel, unrelated to the bar itself but occurring in the same channel belt or as part of laterally amalgamated channel belts. Also, all results relating to the relative thickness of bars and channel fills (Figure 5A-B) might be affected by partial preservation of the architectural elements.

Information on the mean thickness of bars and mud plugs is arguably more meaningful if evaluated by channel complex rather than stratigraphic interval (as given in Figure 5C); however, this was not done because the sample would have been too limited in size.

Database output on the relative thickness of bars and channel fills (Figure 5A-B) indicates that, overall, 20% of the studied bars display characteristics compatible with a scenario of complete compartmentalization. Output on the mean thickness of bars and mud plugs (Figure 5C) suggests that a dominance of full compartmentalization over string-of-beads architecture might be seen in 13% of the stratigraphic intervals considered. On this basis, string-of-beads architectures appear to be prevalent, but bars that are completely compartmentalized might also occur locally, and might dominate in rare occasions.

However, based on database analysis, it is observed that channel complexes that represent meander belts, or the preserved product of the lateral amalgamation of meander belts, display width-to-thickness aspect ratios with mean values of 69.0 and median of 21.7 (range: 4.6-727.3); thus, these units do not commonly represent shoestring sandbodies, which might appear to be implied in the term ‘string-of-beads’.

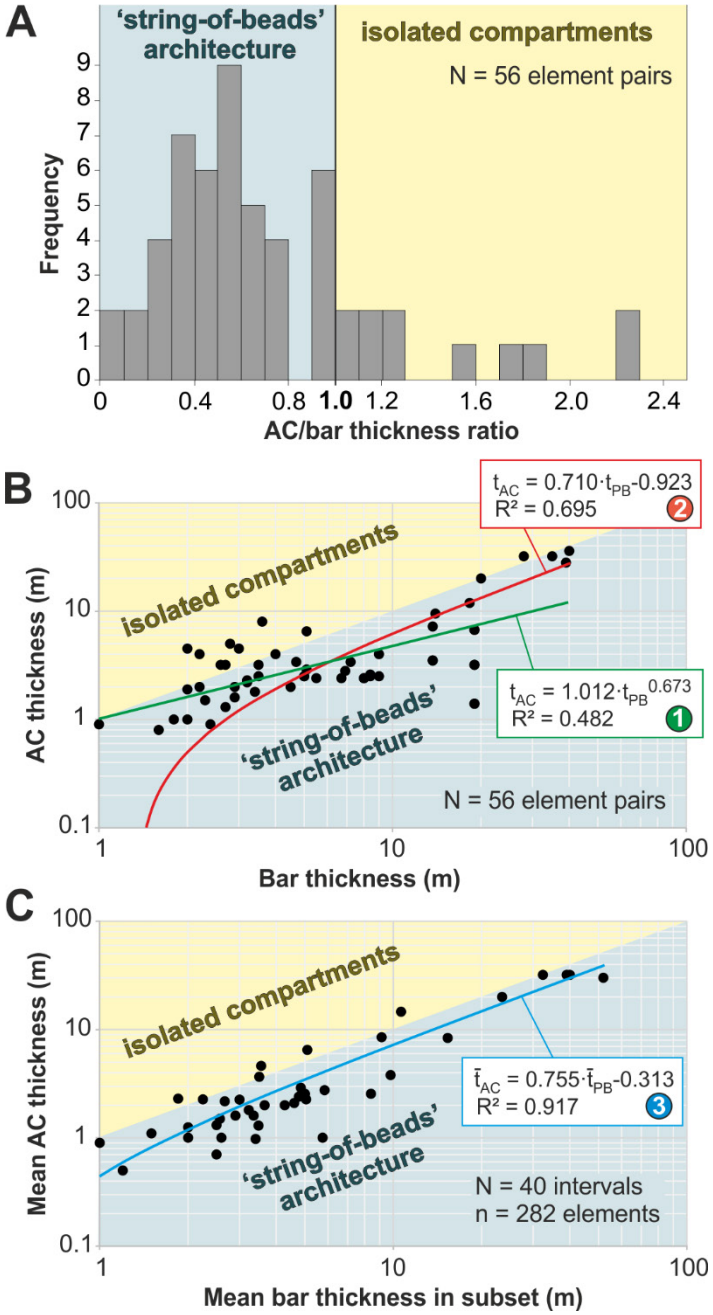

Figure 5. (A) Distribution of the thickness ratio of laterally juxtaposed abandoned-channel fills and point bars or laterally accreting barforms. **(B)** Cross-plot of abandoned-channel-fill thickness vs. bar-form thickness, for pairs of laterally adjacent architectural elements; both linear (red) and power-law (green) relationships have been fitted to the data. **(C)** Cross-plot of mean abandoned-channel-fill thickness vs. mean bar-form thickness, evaluated for stratigraphic intervals; a best-fit linear relationship has been fitted to the data. For each pair of variables, empirical relationships are reported in respective boxes, with associated coefficients of determination.

4.2 Prediction of compartment volumes

Although meander-belt deposits with string-of-beads architectures are characterized by increased sand-to-sand connectivity, relative to channel belts made of isolated bars, they are still fundamentally subject to compartmentalization problems related to the internal arrangement of channel-form and bar-form elements. In particular, where a channel-belt reservoir is capped by floodplain or marine mudstones, the upper portion of the channel belt might develop into a series of 'attic' connections (*sensu* Hovadik & Larue 2007; attic compartments hereafter), which represent portions of point-bar sandbodies at a position higher than the base of the mud plugs. In a scenario of production by waterflooding, it is expected that residual hydrocarbons remain trapped in compartments of this type if bars are not penetrated by any well (Figure 1C). Depending on their volume, untapped hydrocarbons contained in these deposits might justify infill drilling to be undertaken, or the production drive mechanism to be changed. To inform production strategies, it is therefore useful to be able to make predictions concerning the expected volume of reservoir compartments of this type.

To achieve this, firstly, it is important to understand whether the thickness of sands that represent active channel deposition and act as connectors between point-bar sandbodies reflects processes that are scale dependent or not, and so whether the relative thickness of bars and abandoned channel fills is constant or varies systematically with the thickness of the bars, because this dependency could be used predictively.

Regression curves have been fitted to the data in Figure 5, to model relationships between the thickness of bars and the thickness of laterally transitional mud plugs (Figure 5B), and between the average thickness of bars and the average thickness of mud plugs in stratigraphic intervals (Figure 5C). Data relating to pairs of laterally transitional elements have been fitted with both linear and power-law regression curves (Figure 5B); the former, which yields a larger coefficient of determination, predicts an increase in the channel-fill-to-bar-thickness ratio with increasing bar thickness, whereas the latter predicts a decrease in thickness ratio instead (Figure 6). Data relating to the mean thickness of elements in stratigraphic intervals have been fitted with a linear regression curve (Figure 5C), which predicts an increase in the relative thickness of mud plugs and bars with increasing bar thickness (Figure 6). Thus, the two regression curves that provide the best fit to the data in Figure 5 predict an increase in the relative thickness of mud plugs and bars with bar thickness, particularly for bars that are thinner than about 10 m (Figure 6).

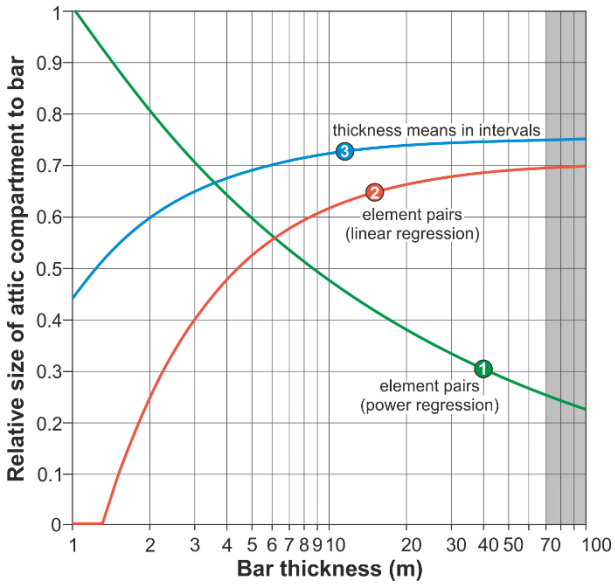

Figure 6. Prediction of the relative thickness of abandoned channel fills and bars as a function of bar thickness, by empirical relationships derived from regression of data in Figure 5B-C. The best-fit relationships for pairs of laterally stacked elements (curve 2, red) and for means in stratigraphic intervals (curve 3, blue) both predict an increase in the relative thickness of mud plugs and bars with bar thickness. The power-law fitted to data relating to pairs of laterally stacked elements (curve 1, green) predicts a decrease in the relative thickness of mud plugs and bars with bar thickness (see Figure 5B). The relative thickness of mud plugs and bars can be taken as a measure of the size of attic compartments. The grey area indicates values of bar thickness that are undocumented (over 70 m).

Employing the three empirical relationships that relate (mean) abandoned-channel-fill thickness to (mean) bar thickness, in combination with expressions that relate the most-likely volume of bars for the three bar-shape types considered in Figure 4 (i.e., as half circular, half elliptic, or crescentic in planform), envelopes of relationships are obtained that can be used to estimate the most-likely volume of attic compartments in a meander belt as a function of (mean) bar thickness (Figure 7). As expected, for most values of bar thickness, the variability in volume estimation seen within each envelope of bar-shape types is limited with respect to the variability seen across these envelopes, in relation to how the relative thickness of bars and mud plugs is modelled (Figure 7).

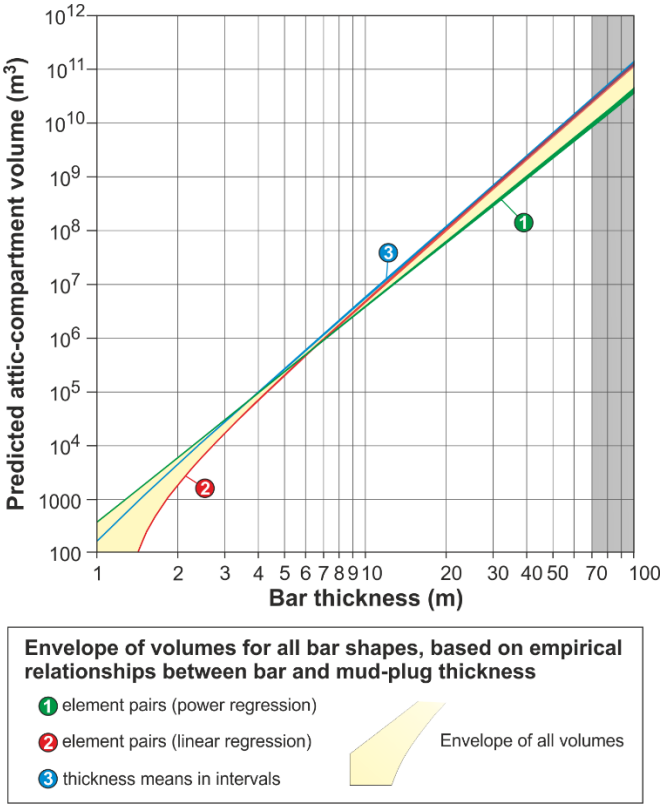

Figure 7. Envelopes of volumes for individual meander-belt attic compartments as predicted from bar thickness, for types of bar planform shapes (half circle, half ellipse, and crescent); the three envelopes are based on the three alternative empirical relationships between mud-plug thickness and bar thickness given in Figure 5; the cumulative envelope of all volume estimates is represented in yellow. The grey area indicates values of bar thickness that are undocumented (over 70 m).

Results in Figure 7 simply relate the gross volume of attic bar compartments. However, analogue information on the facies architecture of bars can be used to attempt estimates of the likely corresponding net volume in data-poor situations (i.e., when direct evaluations on net-to-gross ratios from subsurface datasets are not available). Output from FAKTS presented in Figure 8 describes the distribution in net-to-gross ratio for point bars and/or laterally accreting barforms, based on definition of non-net volumes as consisting of either (i) fine-grained deposits (mud and interlaminated mud and very fine sand; Figure 8A), or (ii) fine-grained and all gravel-sized deposits (Figure 8B), to account for the possible role of mud-clast conglomerates as non-net deposits. On the basis of this information, predictions of net reservoir volumes in attic compartments can be attempted: envelopes that predict the most-likely net volume of attic compartments in a meander belt as a function of bar thickness (or mean bar thickness) are plotted in Figure 9 for a pessimistic scenario, consisting of a net-to-gross ratio equivalent to the 25th centile in the distribution that only considers sands as net deposits (77% net-to-gross ratio). However, these results do not take into consideration the fact that upper point bars, spanning or contained in attic compartments, might display a significantly lower net-to-gross ratio than what is evaluated for the bars in their entirety.

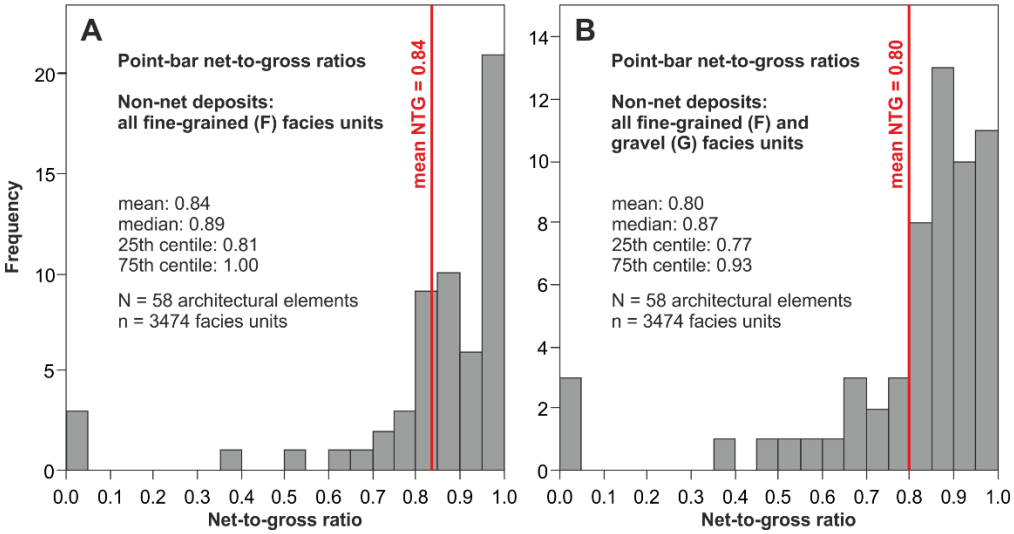

Figure 8. (A) Distribution of net-to-gross ratios for suitable laterally accreting barforms or point bars included in FAKTS, based on measured lithofacies thicknesses, and assuming fine-grained deposits as representing the only non-net volumes. **(A)** Distribution of bar-form net-to-gross ratios, based on measured lithofacies thicknesses, and assuming all fine-grained and gravel deposits as non-net volumes.

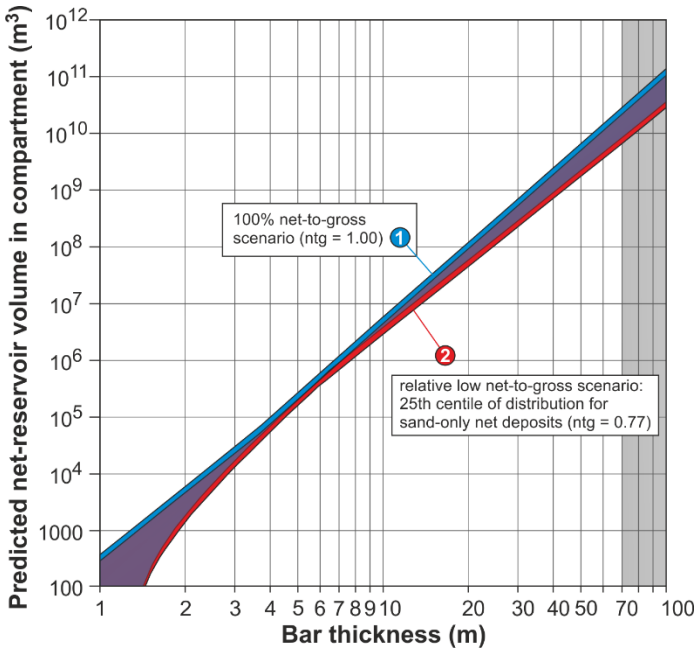

Figure 9. Cumulative envelopes of all estimates of net volumes of meander-belt attic compartments, as functions of bar thickness, and based on all types of bar planform shapes and empirical relationships between mud-plug thickness and bar thickness. The blue envelope (1) reflects a bar-form net-to-gross ratio equal to 100%, whereas the red envelope (2) reflects a bar-form net-to-gross ratio equal to 77% (pessimistic scenario corresponding to the 25th centile in the net-to-gross distribution in Figure 8B). The domain of overlap between the two envelopes appears in purple. The grey area indicates values of bar thickness that are undocumented (over 70 m).

Crucially, estimates of attic-compartment volumes rely on relationships between bar volume and bar thickness, which themselves are based on empirical equations relating bar width to bar thickness, and bar length to bar width (Figure 2C-D). The uncertainty in estimates of the volumes of bars and compartments associated with these empirical relationships is significant. To relate the error that might be associated with volume estimates, power laws that describe relationships between bar width and thickness but that are respectively overly optimistic and pessimistic with respect to the best-fit equation (but with comparable exponent) have been considered; quantities returned by these equations are admissible on the basis of values of bar thickness and width seen in the analogue dataset (Figure 10A). Application of these equations results in predicted volumes for bars (Figure 10B) and attic compartments (Figure 10C) that differ considerably from the base-case predictions made on the basis of the best-fit curves, by over an order of magnitude in the more pessimistic case. This highlights that the way in which bar-form morphometric parameters are predicted has much higher influence than choices on how to model bar shape types or the relative size of bars and channel fills.

5. Suiting well-array configurations to channel-belt geometries

The geometrical organization of a meander-belt reservoir in which point bars can be simplified as tanks of sand and abandonments as impermeable barriers will determine the optimal configuration of a well array employed to produce it. Thus, further empirical characterization of geological analogues is undertaken with the aim to assess the following: (i) relationships between the size of bars and the channel complexes in which they are contained, which offer an estimation of the total lateral extent of meander-belt units; (ii) relationships between the lateral extent of bars and mud plugs, and so the likely horizontal spacing of bars and compartments; (iii) distributions in bar planform area, which find application in probabilistic estimates of the proportion of bars and compartments that may still be unpenetrated by a well array. In addition, the results presented here provide constraints that might help reduce key reservoir uncertainties at the appraisal stage, and assist the creation of static reservoir models.

5.1 Relationships between bar-form size, spacing, and channel-belt extent

Analogue data from FAKTS can be used to elucidate scaling relationships that might exist between bars, associated channel fills, and the channel belts that they form (Figure 11A). Overall, positive scaling is expected between the morphometric parameters of bars, channel fills and channel belts, in part because a channel belt will be at least as wide as the cumulative width of a bar contained in it and of its genetically related channel fill. This positive scaling will primarily reflect river size, and so water discharge (cf. Hickin 1974; Blum et al. 2013), but additional controlling factors on point-bar width will equally control the width of channel complexes; these processes might include for example styles of meander transformation (e.g., preferential meander expansion might act to increase meander-belt width by increasing bar width; cf. El-Mowafy & Marfurt 2016), modes of meander cut-off, or channel migration rates (linked for example to climate-driven changes in sediment supply or to backwater effects; Nanson & Hickin 1983; Fernandes et al. 2016). On the contrary, other types of forcings will be particularly important in determining the preserved geometry of the composite channel complex, but might have only local or limited influence on the geometry of the bars that form it; these controls might include channel-belt avulsion periods, which

determine the timespan allowed for river migration, topographic constraints (e.g., valley confinement, topographic controls on fan-apex locations through their influence on nodal avulsion), and basin subsidence rates, which will control the likelihood of lateral amalgamation of separate inter-avulsion channel belts to form composite bodies.

This type of scaling between bars and channel complexes is seen in FAKTS analogues (Figure 11). To describe this positive scaling, power-law regression curves have been derived that express the relationships between (i) bar and channel-complex width (Figure 11B), (ii) the mean width of bars in a channel complex and the channel-complex width (Figure 11C), and (iii) the mean width of bars and channel complexes in stratigraphic intervals (Figure 11D). Also, empirical equations have been fitted to analogue data to express the relationships between (i) the width of bars and laterally transitional abandoned channel fills (Figure 12A), (ii) the mean width of bars and abandoned channel fills in channel complexes (Figure 12B), and (iii) the mean width of bars and abandoned channel fills in stratigraphic intervals (Figure 12C).

Equations in Figure 11 are applicable to predictions of channel-complex widths from bar width and mean width, which in turn can be predicted by bar thickness and mean thickness (Figures 2C and 3A). For values of bar width over ~300 m, the proposed relationship between channel-complex width and bar width (Figure 11B) offers a more conservative estimate of channel complex width than a prediction of channel-belt width obtained by inverting a corresponding equation compiled by Schenk (1992) on the basis of data from modern rivers.

Equations in Figure 12 are applicable to predictions of the spacing of individual bars in channel belts. The width of abandoned channel fills should approximate the bankfull width of the formative river reach. However, predictions of abandoned-channel element width based on the equation in Figure 12A are smaller than what is computed on the basis of relationships between bar length and channel bankfull width by Yue et al. (2007; Wu et al. 2008), valid for point bars shorter than ~2 km in length, inverted and coupled with relations between bar length and width (Figure 2D); this discrepancy might reflect partial preservation of the original channel forms in the stratigraphic record.

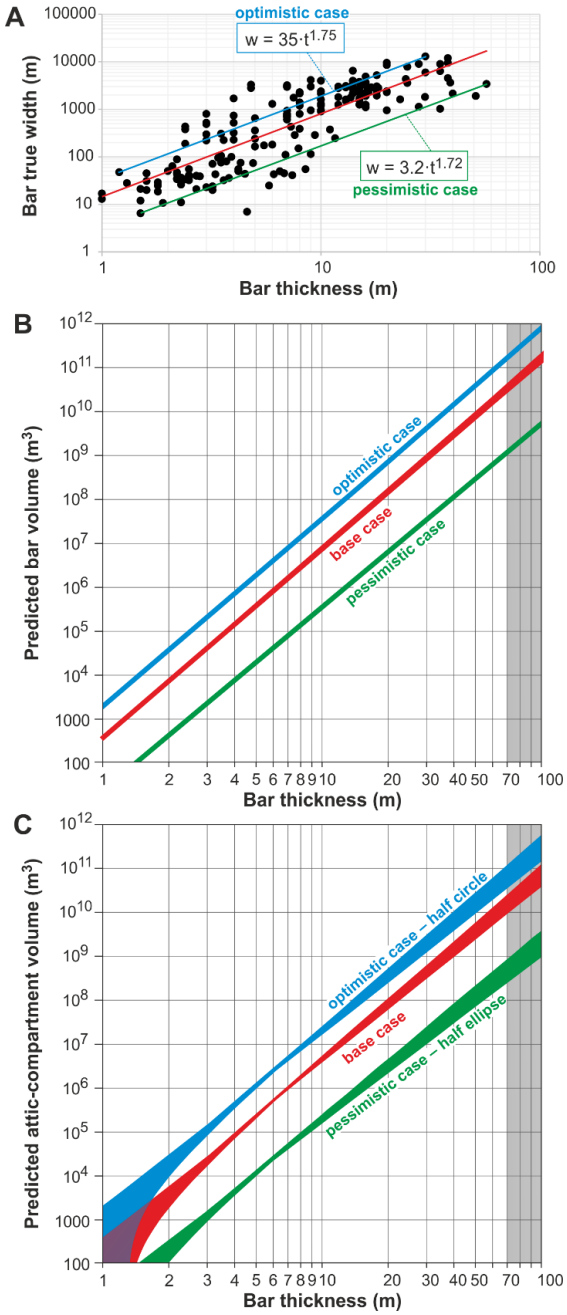

Figure 10. (A) Cross-plot of width vs. thickness for point bars and laterally accreting barforms; the best-fit power-law empirical equation employed in this work (in red) is compared with power-law relationships with similar exponents and contained in the width and thickness domains, but that are overly optimistic (in blue) and pessimistic (in green) with respect to the base case obtained from regression of the data. **(B)** The cumulative envelope of base-case estimates of bar-form volume as predicted from bar thickness, based on three types of bar planform shapes, as given in Figure 4, is represented in red, and is compared with corresponding envelopes obtained by applying predictions of bar-form widths derived using the optimistic (blue) and pessimistic (green) power laws reported in A. **(C)** The cumulative envelope of base-case estimates of meander-belt attic-compartment volume as predicted from bar thickness, based on combinations of types of bar shapes and alternative relationships between mud-plug thickness and bar thickness, as given in Figure 5, is represented in red, and is compared with corresponding envelopes obtained by applying predictions of bar-form widths derived using the optimistic (blue) and pessimistic (green) power laws reported in A. The domain of overlap between the optimistic and base-case envelopes appears in purple. The grey areas indicate values of bar thickness that are undocumented (over 70 m).

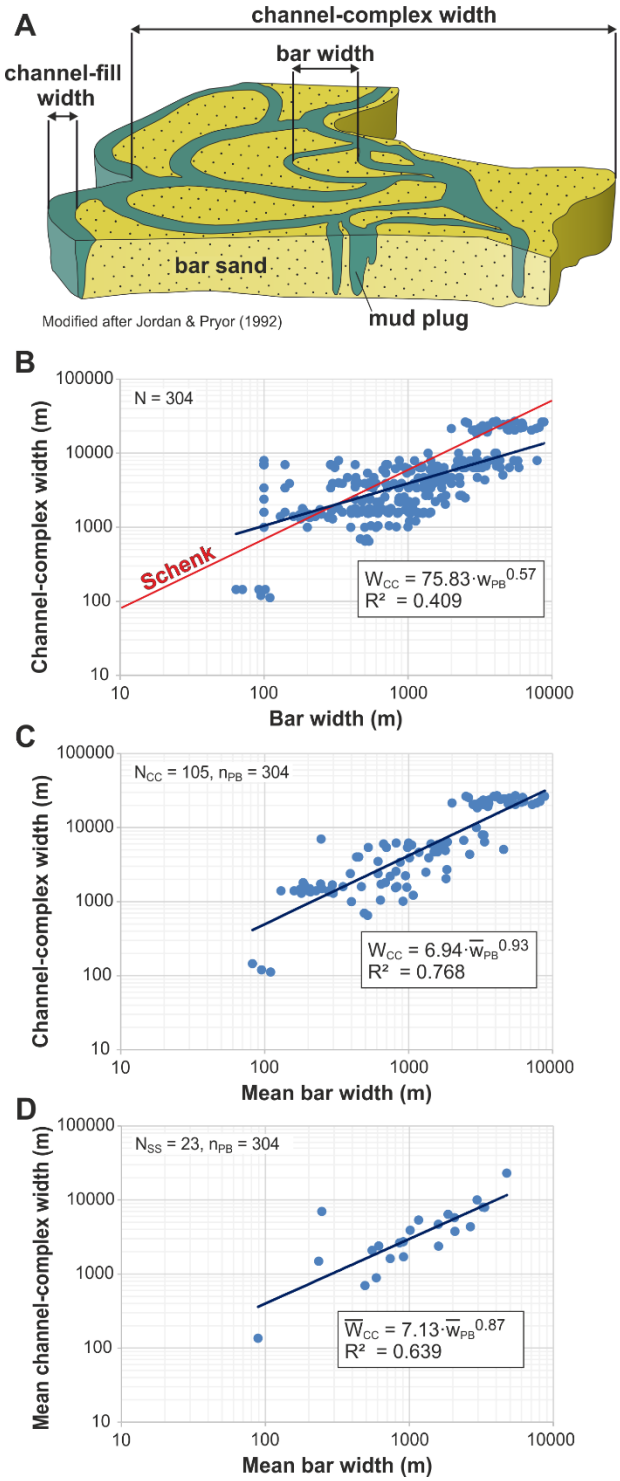

Figure 11. (A) Representation of the width of genetically associated bars, abandoned channel fills, and channel complexes; figure modified after Jordan & Pryor (1992). **(B)** Cross-plot of channel-complex width vs. width of point bars and laterally accreting barforms; a best-fit power-law relationship has been fitted to the data (in blue), and compared with a corresponding relationship by Schenk (1992) (in red). **(C)** Cross-plot of channel-complex width vs. mean width of point bars and laterally accreting barforms; a best-fit power-law relationship has been fitted to the data (in blue). **(D)** Cross-plot of mean channel-complex width vs. mean width of point bars and laterally accreting barforms, evaluated for stratigraphic intervals; a best-fit power-law relationship has been fitted to the data (in blue). For each pair of variables, empirical relationships are reported in respective boxes, with associated coefficients of determination.

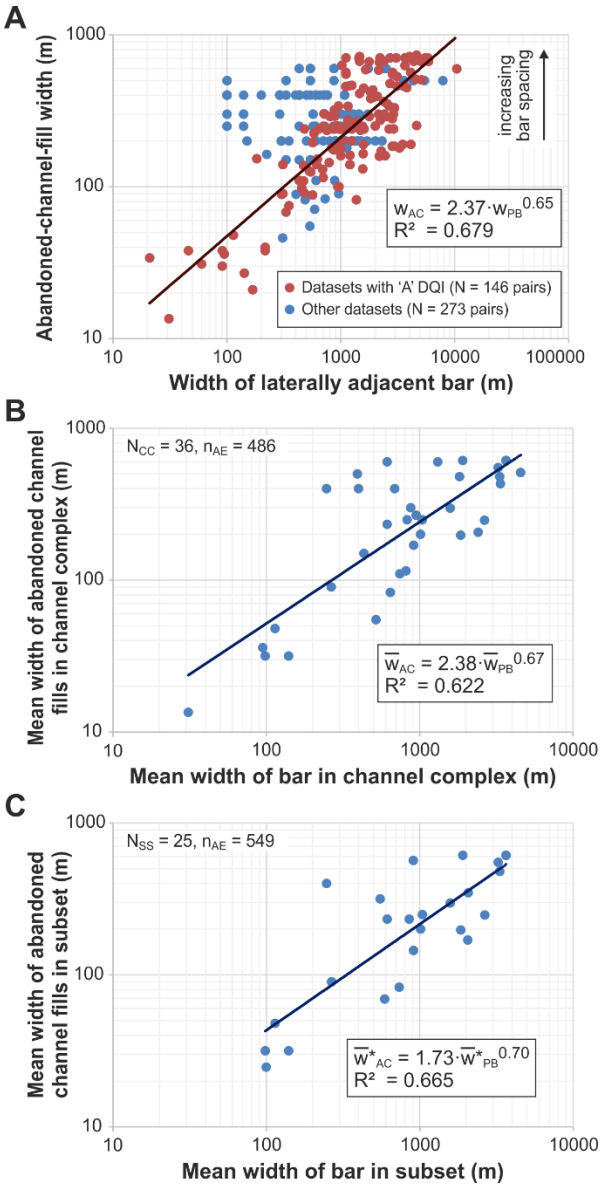

Figure 12. (A) Cross-plot of abandoned-channel-fill width vs. width of point bars and laterally accreting barforms, for pairs of laterally adjacent architectural elements; data from highest-quality datasets (scoring 'A' in data quality index, DQI; Colombera et al. 2012) are represented in red; a best-fit power-law relationship has been fitted to A-DQI data (in red). **(B)** Cross-plot of mean abandoned-channel-fill width vs. mean width of point bars and laterally accreting barforms, evaluated for distinct channel complexes; a best-fit power-law relationship has been fitted to the data (in blue). **(C)** Cross-plot of mean abandoned-channel-fill width vs. mean width of point bars and laterally accreting barforms, evaluated for stratigraphic intervals (subsets); each stratigraphic interval represents either a succession, or parts of it that are conveniently distinguished to describe stratigraphic variations in architecture and/or depositional-system boundary conditions; a best-fit power-law relationship has been fitted to the data (in blue). For each pair of variables, empirical relationships are reported in respective boxes, with associated coefficients of determination.

Predictions of the total extent of channel-complex sandbodies and of the spacing of point bars in it (and relative ranges) permit an assessment of geological characteristics (and associated uncertainties) that might be useful for guiding development and production

planning. In particular, given that perforation of horizontal wells has been suggested and implemented as a way to tackle stratigraphic compartmentalization in meander-belt reservoirs (Schenk 1992; Carter et al. 1998; Pranter et al. 2007; Wu et al. 2008; Harr et al. 2011; Pakdeesirote et al. 2016; Wang et al. 2016), the empirical characterization presented above provides information that is useful for defining the optimal spacing and length of horizontal wells. When dealing with multi-lateral channel bodies, horizontal wells oriented orthogonally to the channel-belt axis (i.e., in the overall cross-stream, or strike, direction) might be suggested, given that point-bar lengths are larger than widths (Figure 2), as this will result in a larger proportion of bars and compartments intersected for a given borehole density. Particularly for a scenario of strike-oriented horizontal wells, it might be useful to consider the likelihood of observing a multi-lateral (*sensu* Pettijohn et al. 1973) channel-complex architecture, characterized by laterally coalescing bars. Analogue data from FAKTS indicate that the percentage of channel complexes that are wider than:

- twice the sum of the average widths of point bars or laterally accreting bars and mud plugs contained in them is 56%,
- three times the sum of the average widths of bars and mud plugs contained in them is 16%.

These numbers might underestimate the degree of multi-lateral organization of the channel complexes, given that the position of overlap for bars that are juxtaposed laterally may not coincide with the position of maximum width. Based on the analysis of 191 strike-directed horizontal architectural-element transitions, ~63% of the point bars or laterally accreting bars in FAKTS are seen to pass laterally to other bars, either through direct juxtaposition (56% of the times) or across a channel-fill element (44% of the times).

The information presented above also has the following applications:

- definition of relative dimensional parameters for sedimentary units that are related hierarchically (channel complexes vs. bars and channel fills) or spatially (adjacent bars and channel fills), for use in stochastic reservoir modelling;
- provision of ranges of reservoir extent from bar-sandstone thickness, which can be considered to advise the drilling of appraisal wells and inform well correlations.

5.2 A probabilistic approach for informing well-array configurations

The aim of this section is to estimate the proportion of individual bars that are intersected by an array of vertical wells, either by an injector or a producer, for given well spacing and point-bar size. This is achieved following a probabilistic approach. Point bars are simplified as discoidal units, i.e., they are considered to have a circular planform shape. Thus, the situation considered represents a general case that ignores planform anisotropy and orientation of the bars, and only applies to non-tilted stratigraphy. To inform the size of these discoidal targets on analogue data, the bars are considered to have a horizontal radius equal to the mean of half their length and half their width (Figure 13A); this is referred to as ‘equivalent radius’ hereafter. Assuming point bars as circular in planform is somewhat unrealistic, but necessary for the following probabilistic treatment. Also, the only case treated is the one of a square grid search with constant well spacing, which is consistent with well arrays with a 5-spot well pattern (Figure 13 B-C). The length of the side of each square (injector-producer distance; Figure 13B-C) is S.

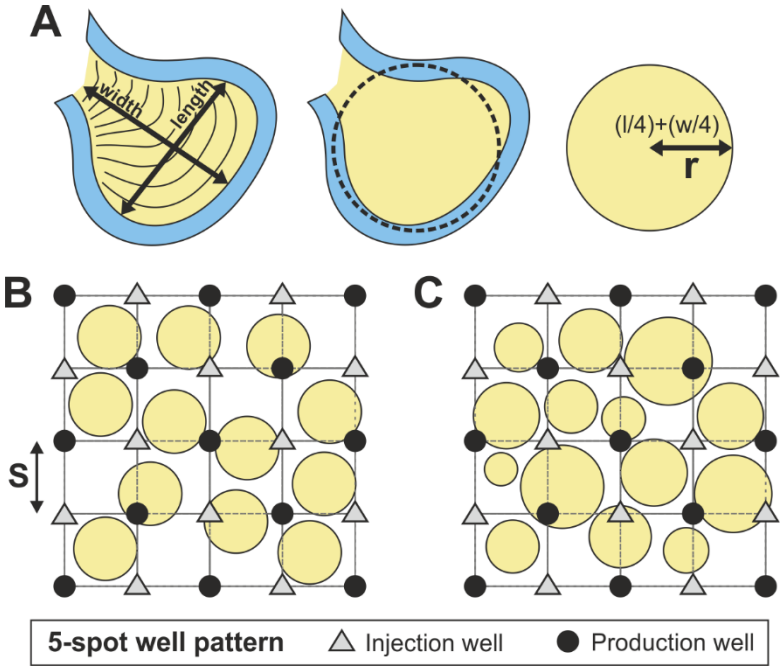

Figure 13. (A) Representation of how the planform shape of point bars is approximated as a circle for analytical purposes, and of how the bar 'equivalent radius' relates to bar width (w) and length (l). **(B)** Plan view of an idealized scenario of a meander-belt sampled by a chessboard square grid, in which bars are simplified as discoidal units and are assumed to have the same radius; the choice of a square grid is compatible with a 5-spot well pattern of injectors and producers; well spacing (S) is defined as the distance between two consecutive wells along a square of the grid (injector-producer separation). **(C)** Plan view of an idealized scenario of a meander-belt sampled by a chessboard square grid, in which bars are simplified as discoidal units with variable radius.

As explained below, a probabilistic estimate of the fraction of bars and compartments penetrated relies on a probability density function that describes analytically the distribution of the bar radius.

Anderson–Darling statistics indicate that the channel complex included in FAKTS with the largest number of bars studied (N = 56; Ganges; Boeser 2011; Figure 14A) has a distribution of the point-bar equivalent radii that is better described by gamma (AD statistic = 0.288, p-value > 0.250), Weibull (AD = 0.272, p-value > 0.250) or lognormal (AD = 0.610, p-value = 0.108) distributions, rather than by a normal one (AD statistic = 1.334, p-value < 0.005). In general, a result of this type might reflect the fact that, although the distribution in size of currently growing bars may be normal along an active reach, larger bars associated with abandoned reaches may be more likely to be partially reworked by subsequent erosion by mobile channels, compared to smaller ones, because they cover larger areas. However, the case examined by Boeser (2011) is the one of a modern channel complex that records lateral amalgamation of different channel belts, associated with rivers of different size and formative discharge, and this is the likely cause for the observed skewness. The Anderson–Darling test applied to a channel complex appearing as a simple meandering channel belt (N = 12; Arang Fm.; Maynard & Murray 2003; Figure 14B) indicates that a normal distribution of

the point-bar equivalent radii might instead be better suited to describe non-amalgamated channel belts (AD = 0.324, p-value > 0.475).

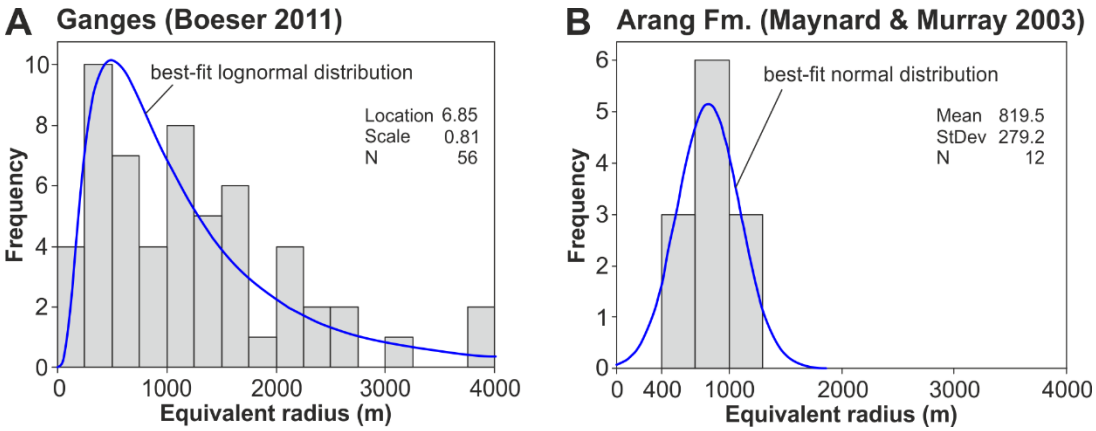

Figure 14. (A) Distribution in equivalent radius for point bars from reaches of the Ganges river system in Bihar (India); a best-fit lognormal distribution is shown. **(B)** Distribution in equivalent radius for point bars of a preserved channel belt in the Upper Arang Formation (Middle Miocene; West Natuna Basin; Sunda Shelf); a best-fit normal distribution is shown.

To provide further information for supporting choices of point-bar size distributions, a geomorphological investigation based on analysis of satellite imagery has been carried out on reaches from 11 rivers that form wide channel belts made of laterally coalescing bars (Fly – Papua New Guinea; Senegal – Senegal; Murray – Australia; Yana – Russia; Colville – USA; Kuskokwim – USA; Mississippi – USA; Amazon – Peru; Irtysh (Ob) – Russia; Kolyma – Russia; Brazos – USA). The area subtended by a meander (as represented in Figure 15A) has been measured for 30 meanders from each of these rivers, whereas data on the width of both meanders and point bars (Figure 15A) are available from 215 channel bends. Meander areas, which are more readily quantified from satellite images than point-bar areas, have been considered as proxies for bar area, based on recognition of the value of the former as a predictor of the latter (Figure 15B). Distributions of meander area have been assessed for the 11 river reaches. Distributions in meander areas are all characterized by positive skewness (cf. four examples in Figure 15C), and apart from one case (Fly River) all the distributions (i) have skewness larger than 1.0 and (ii) are better described by a lognormal curve, rather than a normal bell, based on Anderson–Darling statistics. If a measure comparable to the equivalent radius is derived from the meander area (as the square root of the area divided by π; [m]), the distributions in equivalent radii are seen to (i) show skewness that is positive in all but one case (Fly River), and larger than 1.0 in two cases (Yana and Amazon rivers), and (ii) to be better described by a lognormal curve, rather than a normal one, in all cases, based on Anderson–Darling statistics. These data include readings that relate to both active (N = 215) and abandoned (N = 115) meanders. However, distributions in meander areas for active river bends alone are also better described by a lognormal curve, rather than a normal curve, in all cases except two (Fly and Kolyma rivers), based on Anderson–Darling statistics. Distributions in abandoned-meander areas are better described by a lognormal curve, rather than a normal curve, in all the studied river systems.

This indicates that, even for point bars associated with currently active reaches, positively skewed distributions of bar size may be inherent primary characteristics.

All the studied rivers are characterized by distributions in abandoned-meander areas that have a lower mean than active-meander areas. Based on t-test statistics, whose meaningfulness is affected by the limited size of the sample and non-normality in the data, this difference is statistically significant in two cases at the 0.05 level of significance (Kuskokwim – $T = 2.41$, d.f. = 22, p-value = 0.025; Brazos - $T = 2.34$, d.f. = 15, p-value = 0.034) and in four cases at the 0.10 level of significance (including: Amazon – $T = 1.84$, d.f. = 20, p-value = 0.033; Kolyma – $T = 1.93$, d.f. = 20, p-value = 0.067). There are several possible reasons to explain this difference. For example, it is likely that the difference in size reflects partial erosional obliteration of abandoned loops by mobile rivers. Additionally, these observations might in part relate to a control exerted by the process of meander-bend tightening on the planform area of meanders and associated bars: these areas might be reduced for meanders and bars that have undergone neck cut off, relative to their state at any time prior to cut off when the channel was still active, and its curvature less tight.

Based on these considerations, we infer that normal distributions in point-bar equivalent radius might be indicatively suitable to describe some simple channel belts, but lognormal distributions might be more broadly applicable, and are a preferable choice for multi-lateral or amalgamated meander belts.

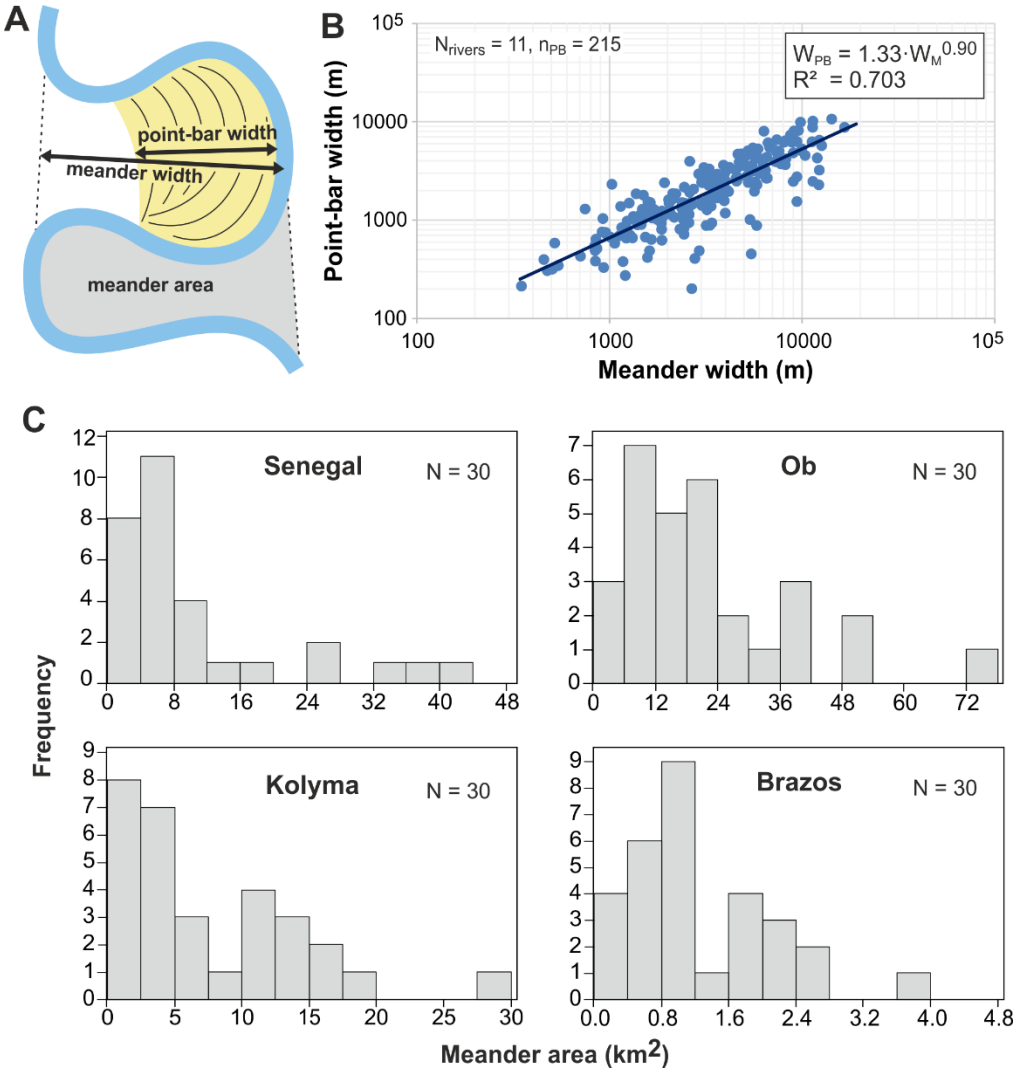

Figure 15. (A) Idealized representation of the relationships between point-bar width, meander width, and meander area, as defined in this work. **(B)** Cross-plot of point-bar width vs. meander width for meander bends from 11 rivers; a power-law empirical relationship that has been fitted to the data is reported with the associated coefficient of determination. **(C)** Distributions in meander area for four of the studied rivers, based on the inclusion of data from both active and abandoned meanders.

The probability that bars with equivalent radius r are intersected at least at one node of the grid (i.e., that at least one well – either injector or producer – penetrates a bar) can be obtained as the probability of detection of circles as given by Shurygin (1976), which is presented here for the particular case of a square chessboard grid and expressed as a function of r:

$$P(p/r) = \begin{cases} \left(\frac{\pi r^2}{S^2}\right) & if\ r \le \frac{S}{2} \\ \left(\frac{2r^2}{S^2}\right)\left[\arcsin\left(\frac{S}{2r}\right) + \left(\frac{S}{2r}\right)\sqrt{1-\left(\frac{S}{2r}\right)^2}\right] & if\ r > \frac{S}{2}, r \le \frac{S\sqrt{5}}{4} \\ \left(\frac{2r^2}{S^2}\right)\left[\arcsin\left(\frac{S}{2r}\right) + \left(\frac{S}{2r}\right)\sqrt{1-\left(\frac{S}{2r}\right)^2} - 2\arccos\left(\frac{S\sqrt{5}}{4r}\right) + \frac{1}{2}\sqrt{\frac{80S^2r^2 - 25S^4}{16r^4}}\right] & if\ r > \frac{S\sqrt{5}}{4}, r \le \frac{S}{2\sqrt{3}-2} \\ 1 & if\ r > \frac{S}{2\sqrt{3}-2} \end{cases}$$

This expression relates the probability of intersecting a bar, i.e., the estimated proportion of intersected bars, given a square grid of given well spacing S (injector-producer distance in a 5-spot well pattern) laid over a meander-belt reservoir in which the size of the bars is constant (case in Figure 13B).

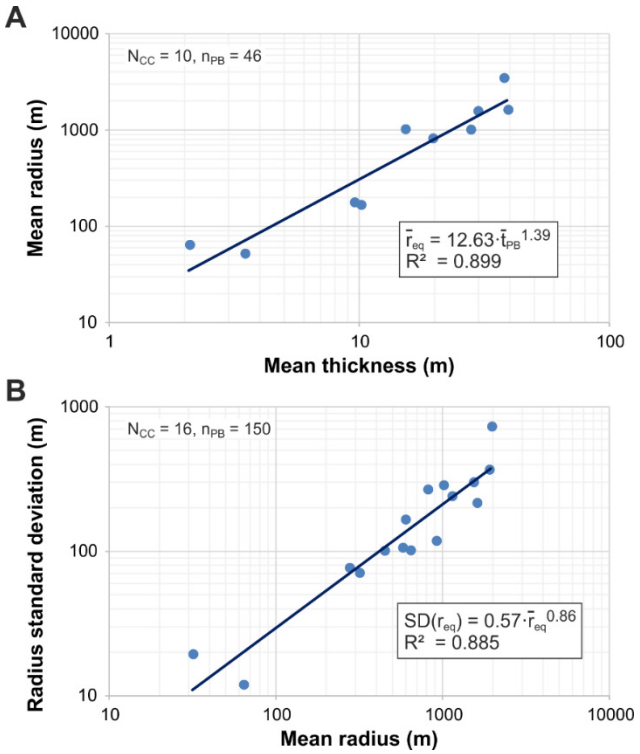

Figure 16. (A) Cross-plot of mean equivalent radius vs. thickness for point bars and laterally accreting barforms, evaluated for individual channel complexes; a power-law empirical relationship has been fitted to the data. **(B)** Cross-plot of standard deviation vs. mean in equivalent radius for point bars and laterally accreting barforms, evaluated for individual channel complexes; a power-law empirical relationship has been fitted to the data. Empirical relationships are reported in boxes, with associated coefficients of determination.

However, it should be noted that for a square grid, the probability that circles with radius r are intersected should only reach 1 for node (well) spacing equal to or smaller than $\sqrt{2}\,r$

(Sinclair 1975). Also, $P(p/r)$ appears as not monotonic on the interval $r > \frac{S\sqrt{5}}{4} < r \leq \frac{S}{2\sqrt{3}-2}$. Upon integration, these facts will respectively determine overestimation and underestimation of total probabilities (see below).

As explained (Figure 13A), for an idealized circular bar, we estimate the equivalent radius as:

$$r = \frac{\left(\frac{w}{2}\right) + \left(\frac{l}{2}\right)}{2}$$

where w and l are the width and length of the actual bar, respectively.

Estimates of the mean and standard deviation of bar radius can be made based on knowledge of mean bar thickness, using equations derived from empirical analysis of FAKTS analogues (Figure 16).

The theorem of total probability is applied to estimate the probability of intersecting a bar (i.e., the estimated proportion of intersected bars) given a square grid of well spacing S laid over a meander belt in which the size of the bars follows a certain distribution (case in Figure 13C).

$P(p/r)$, as given above, is now considered as the conditional probability of point-bar penetration for equivalent radius r. Thus, if the point-bar equivalent radii follow a distribution with a known probability density function $P(r)$, the total probability theorem can be applied:

$$P(p) = \int_{\bar{r}} P(p/r)P(r)dr$$

Thus:

$$\begin{aligned} P(p) = &\int_0^{S/2} \left(\frac{\pi r^2}{S^2}\right) P(r)dr \\ &+ \int_{S/2}^{\frac{S\sqrt{5}}{4}} \left(\frac{2r^2}{S^2}\right) \left[\arcsin\left(\frac{S}{2r}\right) + \left(\frac{S}{2r}\right)\sqrt{1-\left(\frac{S}{2r}\right)^2}\right] P(r)dr \\ &+ \int_{\frac{S\sqrt{5}}{4}}^{\frac{S}{2\sqrt{3}-2}} \left(\frac{2r^2}{S^2}\right) \left[\arcsin\left(\frac{S}{2r}\right) + \left(\frac{S}{2r}\right)\sqrt{1-\left(\frac{S}{2r}\right)^2}\right. \\ &\left. - 2\arccos\left(\frac{S\sqrt{5}}{4r}\right) + \frac{1}{2}\sqrt{\frac{80S^2r^2 - 25S^4}{16r^4}}\right] P(r)dr + \int_{\frac{S}{2\sqrt{3}-2}}^{\infty} P(r)dr \end{aligned}$$

The second and third parts of this expression are not readily integrable; so, a linear approximation of the function will be used (i.e., integration is computed by applying the trapezoidal rule).

Given the problem under consideration, the choice of a probability density function $P(r)$ that describes the distribution of point-bar equivalent radii should be representative of distributions for individual meander belts or amalgamated channel belts, rather than entire

successions or multiple rivers. Based on what was discussed above, to cover different styles of channel-belt organization, we consider the cases of both normal and lognormal distributions in bar size.

If a normal probability density function is assumed suitable to describe $P(r)$, then:

$$P(r) = \left(\frac{1}{\sigma\sqrt{2\pi}}\right)e^{-\frac{(r-\mu)^2}{2\sigma^2}}$$

Where μ is the mean and σ is the standard deviation of the point-bar radius (which can be estimated from knowledge of mean bar thickness based on empirical relationships in Figure 16). Normal distributions are not always appropriate for this purpose, because their domain includes negative values; it is however feasible to consider a normal distribution, applicable to cases of simple channel belts, if the computed total probability reaches 1 for spacing values equal to 0.

If, instead, a lognormal probability density function is assumed suitable to describe $P(r)$, then:

$$P(r) = \left(\frac{1}{rb\sqrt{2\pi}}\right)e^{-\frac{(\ln r-a)^2}{2b^2}}$$

Where a is the location parameter and b is the scale parameter of the distribution of point-bar radii, i.e., the mean and standard deviation of the natural logarithm of the radius, respectively.

Thus, for a meander belt with a family of point bars that have normally distributed sizes, the total probability of point-bar penetration (i.e., the estimated proportion of bars intersected by at least one well) is given by:

$$\begin{aligned}P(p) = &\int_0^{S/2}\left(\frac{\pi r^2}{S^2}\right)\left(\frac{1}{\sigma\sqrt{2\pi}}\right)e^{-\frac{(r-\mu)^2}{2\sigma^2}}dr\\ &+\int_{S/2}^{\frac{S\sqrt{5}}{4}}\left(\frac{2r^2}{S^2}\right)\left[\arcsin\left(\frac{S}{2r}\right)+\left(\frac{S}{2r}\right)\sqrt{1-\left(\frac{S}{2r}\right)^2}\right]\left(\frac{1}{\sigma\sqrt{2\pi}}\right)e^{-\frac{(r-\mu)^2}{2\sigma^2}}dr\\ &+\int_{\frac{S\sqrt{5}}{4}}^{\frac{S}{2\sqrt{3}-2}}\left(\frac{2r^2}{S^2}\right)\left[\arcsin\left(\frac{S}{2r}\right)+\left(\frac{S}{2r}\right)\sqrt{1-\left(\frac{S}{2r}\right)^2}\right.\\ &\left.-2\arccos\left(\frac{S\sqrt{5}}{4r}\right)+\frac{1}{2}\sqrt{\frac{80S^2r^2-25S^4}{16r^4}}\right]\left(\frac{1}{\sigma\sqrt{2\pi}}\right)e^{-\frac{(r-\mu)^2}{2\sigma^2}}dr\\ &+\int_{\frac{S}{2\sqrt{3}-2}}^{r_{MAX}}\left(\frac{1}{\sigma\sqrt{2\pi}}\right)e^{-\frac{(r-\mu)^2}{2\sigma^2}}dr\end{aligned}$$

where μ and σ are the mean and standard deviation of the point-bar radius.

Instead, for a meander belt with point bars that are lognormally distributed in size, the total probability of point-bar penetration (i.e., the estimated proportion of bars intersected by at least one well) is given by:

$$P(p) = \int_0^{S/2} \left(\frac{\pi r^2}{S^2}\right) \left(\frac{1}{rb\sqrt{2\pi}}\right) e^{-\frac{(\ln r - a)^2}{2b^2}} dr$$

$$+ \int_{S/2}^{\frac{S\sqrt{5}}{4}} \left(\frac{2r^2}{S^2}\right) \left[\arcsin\left(\frac{S}{2r}\right) + \left(\frac{S}{2r}\right)\sqrt{1 - \left(\frac{S}{2r}\right)^2}\right] \left(\frac{1}{rb\sqrt{2\pi}}\right) e^{-\frac{(\ln r - a)^2}{2b^2}} dr$$

$$+ \int_{\frac{S\sqrt{5}}{4}}^{\frac{S}{2\sqrt{3}-2}} \left(\frac{2r^2}{S^2}\right) \left[\arcsin\left(\frac{S}{2r}\right) + \left(\frac{S}{2r}\right)\sqrt{1 - \left(\frac{S}{2r}\right)^2}\right.$$

$$\left. - 2\arccos\left(\frac{S\sqrt{5}}{4r}\right) + \frac{1}{2}\sqrt{\frac{80S^2r^2 - 25S^4}{16r^4}}\right] \left(\frac{1}{rb\sqrt{2\pi}}\right) e^{-\frac{(\ln r - a)^2}{2b^2}} dr$$

$$+ \int_{\frac{S}{2\sqrt{3}-2}}^{r_{MAX}} \left(\frac{1}{rb\sqrt{2\pi}}\right) e^{-\frac{(\ln r - a)^2}{2b^2}} dr$$

where a and b are the location and scale parameters of the distribution in point-bar radius.

In both expressions, r_{MAX} is the largest value of equivalent radius for the family of point bars considered.

The second and third parts of both expressions (i.e., the total probabilities for both the normal and lognormal case) are not readily integrable; so, a linear approximation of the function is adopted (integration by trapezoidal rule) to obtain the results presented in this work (Figure 17A).

The relationships obtained by operating the definite integral describe the total probability of penetration of point bars that follow specific probability density functions (e.g., in relation to the size of their formative river) as a function of well spacing S. Relationships of this type are presented in Figure 17A based on application of empirical equations that relate mean and standard deviation of point-bar radius from mean bar thickness (Figure 16), for three chosen values of mean bar thickness (2, 5, and 10 m). The obtained expressions quantify the fractional, not volumetric, proportion of bars that have been intersected by a well array, as a function of well spacing. Hence, results vary significantly depending on the chosen point-bar equivalent radius (Figure 17A). These functions can be employed to predict the proportion of bars that are still unpenetrated, and can be used to estimate volumes of bypassed hydrocarbons, assuming that all (or a predictable fraction of) the unpenetrated bars form attic compartments (as in Figure 1C).

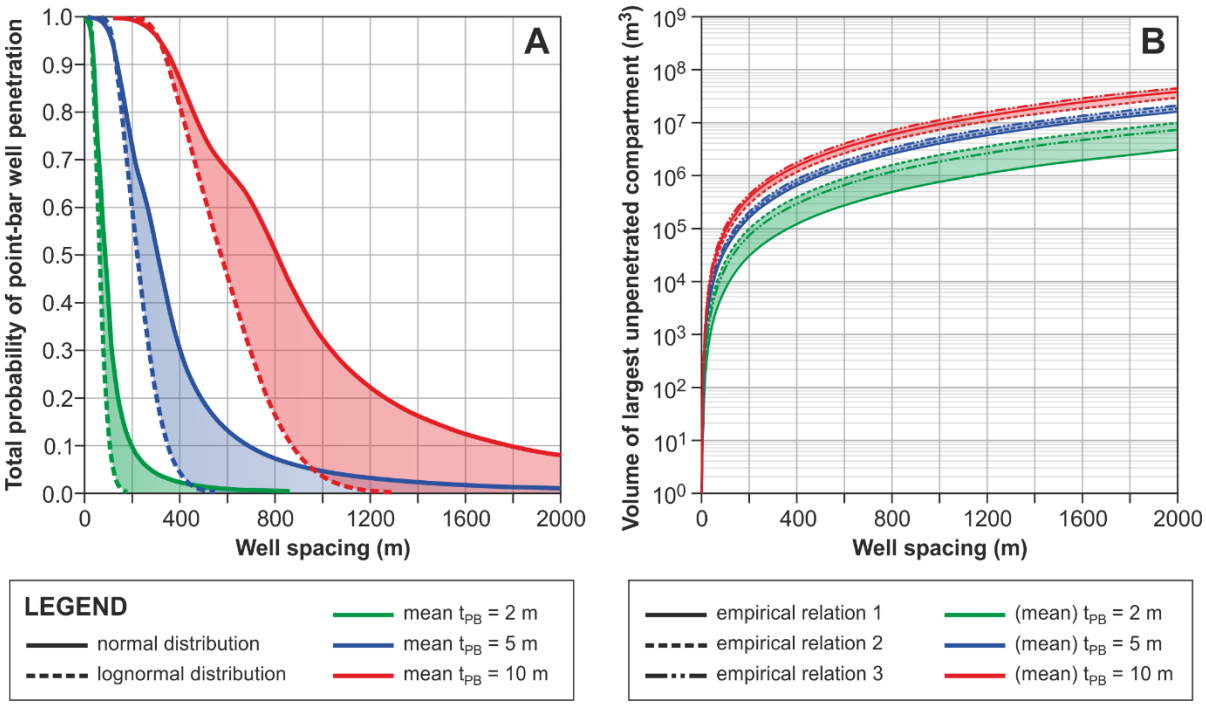

Figure 17. (A) Plots of total probability of point-bar penetration by a square-grid well pattern as a function of well spacing; the graph quantifies the proportion of bars that are likely to have been penetrated by at least one injection or production well, and thus it can be used to derive the proportion of bars that have not yet been intersected by any well. These proportions represent fractions of bars, and not of channel-belt volume. Results are presented for (i) three values of mean bar thickness, on the basis of which mean and standard deviation in bar-form equivalent radius can be estimated by using relationships given in Figure 16, and (ii) for both normal and lognormal point-bar radius distributions. **(B)** Plots of the maximum volume that might be expected for a meander-belt attic compartment that is still unpenetrated by an array of wells with square-grid pattern, based on the assumption of a circular planform shape and on the three alternative empirical relationships between mud-plug thickness and bar thickness given in Figure 5; results are presented for three values of (mean) bar thickness.

Figure 17A shows that meander belts with lognormally distributed bar radii will be sampled less than those with normally distributed radii, for a given well density. Thus, the choice of a lognormal distribution in bar radius will result in a more optimistic prediction of the proportion of meander-belt compartments that are still not intersected by wells. However, in relation to the positive skewness of lognormally distributed radii, it is expected that these compartments will be on average smaller in volume compared to those in the corresponding scenario for normally distributed bar sizes.

Predictions of meander-belt reservoir sampling in terms of well density, applicable to informing infill drilling, can be further supported by estimates of the maximum size of potential bypassed oil pools. The largest possible radius for a circular target that is not intersected by a well array with spacing S is equal to $S/\sqrt{2}$ (Sinclair 1975). It is therefore possible to employ relationships that describe the relative thickness of bars and associated mud plugs (Figure 5B-C) to predict the maximum admissible volume of the unpenetrated attic compartment with largest planform area, as a function of bar thickness. These relationships are presented in Figure 17B for three values of bar thickness (2, 5, and 10 m).

6. Summary, limitations, and other applications

Through a quantitative characterization of sixty-four outcrop, modern, and subsurface geological analogues, a description of the bar-form and channel-form architecture of meander belts has been derived that offers constraints applicable in contexts of hydrocarbon exploration, appraisal, development, and production, for corresponding reservoirs.

Particular focus has been placed on intra-channel-belt compartmentalization by fine-grained abandonment deposits, with the particular scope of providing quantitative information for optimizing the sweep efficiency of programmes of enhanced oil recovery. A number of tools exist for assessing compartmentalization in producing reservoirs (e.g., seismic amplitude vs. offset analysis, geochemical data, pressure analysis, tracer injection; cf. Smalley & Hale 1996; Calvert 2005; Páez et al. 2010). Yet, it is claimed that the diagnosis of compartmentalization in early stages of field development likely improves management throughout a field lifecycle (Smalley & Hale 1996; Fox & Bowman 2010; Smalley & Muggeridge 2010): hence, there is need for empirical knowledge of reservoir architectures that can be used to make pre-drill predictions and to inform development plans. The quantitative tools presented here serve this purpose for meander-belt reservoirs.

Results of the analysis of the chosen analogues are summarized in the following list.

- Relationships between morphometric parameters of bar-form elements, and descriptive statistics thereof for channel belts and study intervals, have been assessed and described by empirical equations.

- The relative geometries of bars and mud plugs have been quantified to determine the likelihood of different styles of compartmentalization of channel belts, which appear to typically take the form of patchworks of bars dominantly connected by thalweg sands (cf. ‘string-of-beads’, *sensu* Donselaar & Overeem 2008) and locally isolated by mud plugs.

- Based on morphometric analyses and geometrical modelling of point-bar geometries, typical volumes associated with bar-scale attic compartments in meander-belt reservoirs or with potential stratigraphic traps have been quantified.

- Information on the relationships between the width of bars, abandonments, and the channel complexes in which they are contained has been derived.

- On the basis of the results from the morphometric analyses, models founded on principles of geometric probability have been proposed for predictions of the proportion of bars and the potential volume of the largest compartments that have not yet been intersected by a well array, expressed as functions of well spacing.

It has been shown that these results provide quantitative constraints for guiding development and production strategies in meander-belt reservoirs, particularly concerning optimal well spacing and orientation and the potential reserve increase driven by infill drilling. Implications and applications of the results have been discussed already, and will not be repeated here. However, there are some limitations that should be considered when applying the insight derived from these results. Some key limitations to the applicability of these results are summarized as follows.

- Attic compartments that might contain bypassed hydrocarbons include point-bar tops, which often are more mud-prone than lower bars and display lower net-to-gross ratios (cf. Miall 1996, and references therein).
- Mud drapes and mud-clast conglomerates that mantle point-bar accretion surfaces commonly act as barriers to flow, and in some cases might partition individual bars into a number of discrete compartments (cf. Pranter et al. 2007; Musial et al. 2013). The compartmentalization imparted by heterolithic packages and laterally continuous mud drapes (cf. Thomas et al. 1987), which is especially important in upper-bar deposits, has been ignored. Analogue data can be useful to assess facies-scale compartmentalization, through geometrical characterization and by conditioning modelling approaches; this topic will represent the focus of future work.
- Bar-to-bar connectivity due to erosional cross-cutting has not been considered, and this likely results in the underestimation of the proportion of intersected compartments (overestimation of untapped compartments) by a well array. Lateral juxtaposition of bars is documented in FAKTS, in which 27% (N = 244) of horizontal transitions within channel belts involving point bars or laterally accreting barforms are seen to occur to architectural elements of the same type. The development of bar-to-bar connections will in part reflect channel-belt morphodynamic behaviours (e.g., processes of neck cut off are likely to generate different compartment geometries compared to chute cut off, and the latter might be more likely to favour bar-to-bar connectivity), but geological controls on bar connectivity still need to be explored.
- Channel forms that are entirely or mostly filled with sand-prone deposits and are interpreted to represent active-channel sedimentation are relatively common constituents of preserved channel-belt architectures; these units might be genetically related to point-bar deposits (e.g., Hubbard et al. 2011) or record a subsequent evolution of river channels (e.g., Corbeanu et al. 2004); their presence will increase sandstone connectivity. Understanding of the controls on their infill and preservation is poor, and requires further investigation.
- Abandoned channel fills may contain sandy beds, which might be emplaced as a consequence of flood deposition; these deposits might enhance connectivity between bars, depending on their geometry. An assessment of the internal lithological organization of abandoned channel fills is warranted.
- The importance of permeability contrasts in meander-belt deposits, and their potential control on dynamic connectivity (*sensu* Renard & Allard 2013) through the occurrence of thief zones, have not been considered in this study. Analogue data on facies geometries and petrophysical properties can be used to assess facies-scale dynamic connectivity through numerical modelling approaches; this topic will be the subject of future work.

The results presented here are specifically relevant to successions in which channel belts are produced by sinuous meandering rivers. Although problems of compartmentalization by abandonment deposits are also seen in deposits interpretable as the product of braided or single-thread low-sinuosity rivers (cf. Lynds & Hajek 2006; McKie 2011), it must be noted that the morphometry and scaling relationships of bars, channel fills and channel bodies produced by braided rivers are fundamentally different from what is described here (cf. Gibling 2006; Kelly 2006; Colombera et al. 2013; Holzweber et al. 2014).

The proposed empirical description of meander-belt geometries and connectivity can also be employed in applications that require characterizing the architecture and connectivity of

aquifers of fluvial origin. This is particularly significant because groundwater aquifers hosted in point-bar sands are widely reported to be systematically subject to arsenic contamination, in relation to the combined role of clay plugs as sources of arsenic and of point bars as traps for contaminants (cf. Desbarats et al. 2014; Donselaar 2014; Donselaar et al. 2017; and references therein). The information in the current work provides measures with which to understand and predict connectivity length-scales and contaminant mobility, and to inform aquifer clean-up programmes, especially those implemented through pump-and-treat remediation (Mackay & Cherry 1989; Testa & Winegardner 2000). The empirical knowledge presented herein is also applicable to predictions of the sedimentary heterogeneity that (i) dictates the optimal configuration of geothermal doublets in fluvial hot sedimentary aquifers (cf. Hamm & Lopez 2012; Crooijmans et al. 2016; Willems et al. 2017), and (ii) controls CO_2 injectivity, migration pathways and storage capacity of meander-belt sandstones targeted for carbon-dioxide capture and storage (cf. Ambrose et al. 2008; Lu et al. 2012).

Acknowledgements

The FRG-ERG sponsors (Areva, BHP Billiton, ConocoPhillips, Det norske oljeselskap ASA (Detnor), Murphy Oil Corporation, Nexen, Petrotechnical Data Systems, Saudi Aramco, Shell, Tullow Oil, Woodside, and YPF) are acknowledged for financial support. LC has been supported by NERC (Catalyst Fund award NE/M007324/1; Follow-on Fund NE/N017218/1). We thank two anonymous reviewers for their constructive comments.

References

Allen, J. R. L. (1984). Sedimentary structures, their character and physical basis, vol. 2. Developments in Sedimentology, 30. Elsevier, Amsterdam. 664 pp.

Alpak, F. O., & Barton, M. D. (2014). Dynamic impact and flow-based upscaling of the estuarine point-bar stratigraphic architecture. Journal of Petroleum Science and Engineering, 120, 18-38.

Ambrose, W. A. (1991). Facies heterogeneity, pay continuity, and infill potential in barrier-island, fluvial, and submarine-fan reservoirs: examples from the Texas Gulf Coast and Midland Basin. In: Miall, A. D., Tyler, N. (eds.), The three-dimensional facies architecture of terrigenous clastic sediments and its implications for hydrocarbon discovery and recovery. SEPM (Society for Sedimentary Geology) Concepts in Sedimentology and Paleontology 3, 13-21.

Ambrose, W. A., Lakshminarasimhan, S., Holtz, M. H., Nunez-Lopez, V., Hovorka, S. D., & Duncan, I. (2008). Geologic factors controlling CO2 storage capacity and permanence: case studies based on experience with heterogeneity in oil and gas reservoirs applied to CO2 storage. Environmental Geology, 54, 1619-1633.

Anderson, D. S. (2005). Architecture of crevasse splay and point-bar bodies of the nonmarine Iles Formation north of Rangely, Colorado: implications for reservoir description. The Mountain Geologist, 42, 109-122.

Berg, R. R. (1968). Point-bar origin of Fall River Sandstone reservoirs, northeastern Wyoming. AAPG Bulletin, 52, 2116-2122.

Blum, M. (2012). Scaling relationships in fluvial systems: implications for the Mannville Group, Alberta Foreland Basin. AAPG Search and Discovery article #51132.

Blum, M. D., & Hattier-Womack, J. (2009). Climate change, sea-level change, and fluvial sediment supply to deepwater depositional systems. In: Kneller, B. C., McCaffrey, W. D., Martinsen, O. J. (eds.), External controls on deep water depositional systems, SEPM Special Publication, 92, 15-39.

Blum, M., Martin, J., Milliken, K., & Garvin, M. (2013). Paleovalley systems: insights from Quaternary analogs and experiments. Earth-Science Reviews, 116, 128-169.

Berg, R. R. (1981). Exploration for sandstone stratigraphic traps. AAPG Continuing Education Course Note Series 3, Third Edition. 47 pp.

Boeser, D. M. (2011). Point bars and clay plugs surface map near Patna (Bihar, India) along the Ganga River. B.Sc. Thesis, Delf University of Technology. 20 pp.

Bridge, J. S., Alexander, J., Collier, R. E., Gawthorpe, R. L., & Jarvis, J. (1995). Ground-penetrating radar and coring used to study the large-scale structure of point-bar deposits in three dimensions. Sedimentology, 42, 839-852.

Busch, D. A., 1974, Stratigraphic traps in sandstones – exploration techniques. AAPG Memoir 21. 164 pp.

Cain, S. (2009). Sedimentology and stratigraphy of a terminal fluvial fan system: the Permian Organ Rock Formation, South East Utah. Doctoral dissertation, Keele University. 359 pp.

Calvert, R. (2005). Insights and methods for 4D reservoir monitoring and characterization. SEG/EAGE Distinguished Instructor Series, 8. 234 pp.

Carter, D. C., Kortlang, W., Smelcer, M., & Troncoso, J. C. (1998). An integrated approach to horizontal well design and planning in Widuri Field, offshore southeast Sumatra, Indonesia. Indonesia. Indonesian Petroleum Association, 30th Annual Convention Proceedings, vol. 2, 135-162.

Carter, D. C. (2003). 3-D seismic geomorphology: insights into fluvial reservoir deposition and performance, Widuri field, Java Sea. AAPG Bulletin, 87, 909-934.

Catuneanu, O., & Bowker, D. (2001). Sequence stratigraphy of the Koonap and Middleton fluvial formations in the Karoo foredeep South Africa. Journal of African Earth Sciences, 33, 579-595.

Catuneanu, O., & Elango, H. N. (2001). Tectonic control on fluvial styles: the Balfour Formation of the Karoo Basin, South Africa. Sedimentary Geology, 140, 291-313.

Chapin, M. A., & Meyer, D. F. (1991). Constructing a three-dimensional rock-property model of fluvial sandstones in the Peoria field, Colorado. In: Miall, A. D., Tyler, N. (eds.), The three-dimensional facies architecture of terrigenous clastic sediments and its implications for hydrocarbon discovery and recovery. SEPM (Society for Sedimentary Geology) Concepts in Sedimentology and Paleontology 3, 160-171.

Colombera, L., Mountney, N. P., & McCaffrey, W. D. (2012). A relational database for the digitization of fluvial architecture concepts and example applications. Petroleum Geoscience, 18, 129-140.

Colombera, L., Mountney, N. P., & McCaffrey, W. D. (2013). A quantitative approach to fluvial facies models: methods and example results. Sedimentology, 60, 1526-1558.

Colombera, L., Mountney, N. P., Felletti, F., & McCaffrey, W. D. (2014). Models for guiding and ranking well-to-well correlations of channel bodies in fluvial reservoirs. AAPG Bulletin, 98(10), 1943-1965.

Colombera, L., Mountney, N. P., Howell, J. A., Rittersbacher, A., Felletti, F., & McCaffrey, W. D. (2016). A test of analog-based tools for quantitative prediction of large-scale fluvial architecture. AAPG Bulletin, 100, 237-267.

Corbeanu, R. M., Wizevich, M. C., Bhattacharya, J. P., Zeng, X., & McMechan, G. A. (2004). Three-dimensional architecture of ancient lower delta-plain point bars using ground-penetrating radar, Cretaceous Ferron Sandstone, Utah. In: Chidsey T. C. Jr., Adams R. D., Morris T. H. (eds.), Regional to wellbore analog for fluvial-deltaic reservoir modeling: the Ferron Sandstone of Utah, American Association of Petroleum Geologists, Studies in Geology, 50, 427-449.

Cornish, F. G. (1984). Fluvial environments and paleohydrology of the Upper Morrow 'A' (Pennsylvanian) meander belt sandstone, Beaver County, Oklahoma. The Shale Shaker, 34, 70-80.

Crooijmans, R. A., Willems, C. J. L., Nick, H. M., & Bruhn, D. F. (2016). The influence of facies heterogeneity on the doublet performance in low-enthalpy geothermal sedimentary reservoirs. Geothermics, 64, 209-219.

Cuevas Gozalo, M. C., & Martinius, A. W. (1993). Outcrop data-base for the geological characterization of fluvial reservoirs: an example from distal fluvial fan deposits in the Loranca Basin, Spain. In: North C. P., Prosser D. J. (eds.), Geological Society, London, Special Publications, 73, 79-94.

De Rooij, M., Corbett, P. W., & Barens, L. (2002). Point bar geometry, connectivity and well test. First Break, 20, 755-763.

Desbarats, A. J., Koenig, C. E. M., Pal, T., Mukherjee, P. K., & Beckie, R. D. (2014). Groundwater flow dynamics and arsenic source characterization in an aquifer system of West Bengal, India. Water Resources Research, 50, 4974-5002.

Donselaar, M. E. (2014). Dissolution and entrapment of arsenic in fluvial point bars—case study of the Ganges River, Bihar, India. In: Litter, M. I., Nicolli, H. B., Meichtry, M., Quici, N., Bundschuh, J., Bhattacharya, P., Naidu, R. (eds.), One century of the discovery of arsenicosis in Latin America (1914-2014) As2014, Proceedings of the 5th International Congress on Arsenic in the Environment, May 11-16, 2014, Buenos Aires, Argentina, Taylor & Francis, London, 26-28.

Donselaar, M. E., & Overeem, I. (2008). Connectivity of fluvial point-bar deposits: An example from the Miocene Huesca fluvial fan, Ebro Basin, Spain. AAPG Bulletin, 92, 1109-1129.

Donselaar, M. E., Bhatt, A. G., & Ghosh, A. K. (2017). On the relation between fluvio-deltaic flood basin geomorphology and the wide-spread occurrence of arsenic pollution in shallow aquifers. Science of the Total Environment, 574, 901-913.

Edie, R. W., & Andrichuk, J. M. (2003). Meander belt entrapment of hydrocarbons at Saddle Lake, Alberta and an untested in situ combustion scheme for recovery of heavy oil. Bulletin of Canadian Petroleum Geology, 51, 253-274.

Edie, R. W., & Andrichuk, J. M. (2005). Meander Belt Entrapment of Hydrocarbons, Campbell-Namao Field, Alberta. AAPG Search and Discovery article #20027.

El-Mowafy, H. Z., & Marfurt, K. J. (2016). Quantitative seismic geomorphology of the middle Frio fluvial systems, south Texas, United States. AAPG Bulletin, 100, 537-564.

Ethridge, F. G., & Schumm, S. A. (1977). Reconstructing paleochannel morphologic and flow characteristics: methodology, limitations, and assessment. In: Miall, A.D. (ed.), Fluvial Sedimentology, Canadian Society of Petroleum Geologists, Memoir 5, 703-721.

Fabuel-Perez, I., Hodgetts, D., & Redfern, J. (2009a). A new approach for outcrop characterization and geostatistical analysis of a low-sinuosity fluvial-dominated succession using digital outcrop

models: Upper Triassic Oukaimeden Sandstone Formation, central High Atlas, Morocco. AAPG Bulletin, 93, 795-827.

Fabuel-Perez, I., Redfern, J., & Hodgetts, D. (2009b). Sedimentology of an intra-montane rift-controlled fluvial dominated succession: the Upper Triassic Oukaimeden Sandstone Formation, Central High Atlas, Morocco. Sedimentary Geology, 218, 103-140.

Fachmi, M., & Wood, L. J. (2005). Seismic geomorphology: a study from West Natuna Basin, Indonesia. Indonesian Petroleum Association, 30th Annual Convention Proceedings, vol. 1, 163-178.

Feng, Z. Q. (2000). An investigation of fluvial geomorphology in the Quaternary of the Gulf of Thailand, with implications for river classification. Doctoral dissertation, University of Reading. 198 pp.

Ferguson, R. J., & Brierley, G. J. (1999). Levee morphology and sedimentology along the lower Tuross River, south-eastern Australia. Sedimentology, 46, 627-648.

Fernandes, A. M., Törnqvist, T. E., Straub, K. M., & Mohrig, D. (2016). Connecting the backwater hydraulics of coastal rivers to fluvio-deltaic sedimentology and stratigraphy. Geology, G37965-1.

Fielding, C. R., Falkner, A. J., & Scott, S. G. (1993). Fluvial response to foreland basin overfilling; the late Permian Rangal Coal Measures in the Bowen basin, Queensland, Australia. Sedimentary Geology, 85, 475-497.

Fisk, H. N. (1947). Fine-grained alluvial deposits and their effects on Mississippi River activity. Volumes 1 & 2. U.S. Corps of Engineers, Mississippi River Commission, Waterways Experiment Station, Vicksburg, MS. 82 + 74 pp.

Ford, G. L., & Pyles, D. R. (2014). A hierarchical approach for evaluating fluvial systems: Architectural analysis and sequential evolution of the high net-sand content, middle Wasatch Formation, Uinta Basin, Utah. AAPG Bulletin, 98, 1273-1304.

Fox, R. J., & Bowman, M. B. J. (2010). The challenges and impact of compartmentalization in reservoir appraisal and development. In: Jolley, S. J., Fisher, Q. J., Ainsworth, R. B., Vrolijk, P. J., & Delisle, S. (eds.), Reservoir compartmentalization. Geological Society, London, Special Publications, 347, 9-23.

Galloway, W. E., & Hobday, D. K. (1996). Terrigeneous clastic depositional systems, Springer-Verlag, Berlin, 489 pp.

Geehan, G., & Underwood, J. (1993). The use of length distributions in geological modelling. In: Flint, S. S., Bryant, I. D. (eds.), The geological modelling of hydrocarbon reservoirs and outcrop analogues, Special Publication of the International Association of Sedimentologists, 15, 205-212.

Ghinassi, M., Billi, P., Libsekal, Y., Papini, M., & Rook, L. (2013). Inferring fluvial morphodynamics and overbank flow control from 3D outcrop sections of a Pleistocene point bar, Dandiero Basin, Eritrea. Journal of Sedimentary Research, 83, 1066-1084.

Gibling, M. R. (2006). Width and thickness of fluvial channel bodies and valley fills in the geological record: a literature compilation and classification. Journal of Sedimentary Research, 76, 731-770.

Guccione, M. J., Burford, M. F., & Kendall, J. D. (1999). Pemiscot Bayou, a large distributary of the Mississippi River and a possible failed avulsion. In: Smith, N. D., Rogers, J. (eds.), Fluvial Sedimentology VI, Special Publication of the International Association of Sedimentologists, 28, 211-220.

Hamm, V., & Lopez, S. (2012). Impact of fluvial sedimentary heterogeneities on heat transfer at a geothermal doublet scale. Proceedings of the thirty-seventh Workshop on geothermal reservoir engineering, Stanford University, Stanford, CA. SGP-TR-194.

Harr, M. S., Chokasut, S., Bhuripanyo, C., Viriyasittigun, P., & Harun, A. R. (2011). Evaluation of factors in horizontal well recovery in the Pattani Basin in the Gulf of Thailand. International Petroleum Technology Conference, IPTC 14981.

Hickin, E. J. (1974). The development of meanders in natural river-channels. American Journal of Science, 274, 414-442.

Hirst, J. P. P. (1991). Variations in alluvial architecture across the Oligo-Miocene Huesca fluvial system, Ebro Basin, Spain. In: Miall, A. D., Tyler, N. (eds.), The three-dimensional facies architecture of terrigenous clastic sediments and its implications for hydrocarbon discovery and recovery. SEPM (Society for Sedimentary Geology) Concepts in Sedimentology and Paleontology 3, 111-121.

Holzweber, B. I., Hartley, A. J., & Weissmann, G. S. (2014). Scale invariance in fluvial barforms: implications for interpretation of fluvial systems in the rock record. Petroleum Geoscience, 20, 211-224.

Hornung, J., & Aigner, T. (1999). Reservoir and aquifer characterization of fluvial architectural elements: Stubensandstein, Upper Triassic, southwest Germany. Sedimentary Geology, 129, 215-280.

Hubbard, S. M., Smith, D. G., Nielsen, H., Leckie, D. A., Fustic, M., Spencer, R. J., & Bloom, L. (2011). Seismic geomorphology and sedimentology of a tidally influenced river deposit, Lower Cretaceous Athabasca oil sands, Alberta, Canada. AAPG Bulletin, 95, 1123-1145.

Ielpi, A., & Ghinassi, M. (2014). Planform architecture, stratigraphic signature and morphodynamics of an exhumed Jurassic meander plain (Scalby Formation, Yorkshire, UK). Sedimentology, 61, 1923-1960.

Jablonski, B. V. J. (2012). Process sedimentology and three-dimensional facies architecture of a fluvially dominated, tidally influenced point bar: Middle McMurray Formation, Lower Steepbank River area, northeastern Alberta, Canada. M.Sc. Thesis, Queen's University, Kingston. 371 pp.

Jackson II, R. G. (1981). Sedimentology of muddy fine-grained channel deposits in meandering streams of the American Middle West. Journal of Sedimentary Petrology, 51, 1169-1192.

Jiao, Y., Yan, J., Li, S., Yang, R., Lang, F., & Yang, S. (2005). Architectural units and heterogeneity of channel reservoirs in the Karamay Formation, outcrop area of Karamay oil field, Junggar basin, northwest China. AAPG Bulletin, 89, 529-545.

Jo, H. R. (2003). Depositional environments, architecture, and controls of Early Cretaceous non-marine successions in the northwestern part of Kyongsang Basin, Korea. Sedimentary Geology, 161, 269-294.

Jolley, S. J., Fisher, Q. J., & Ainsworth, R. B. (2010). Reservoir compartmentalization: an introduction. In: Jolley, S. J., Fisher, Q. J., Ainsworth, R. B., Vrolijk, P. J., & Delisle, S. (eds.), Reservoir compartmentalization. Geological Society, London, Special Publications, 347, 1-8.

Jones, S. J., Frostick, L. E., & Astin, T. R. (2001). Braided stream and flood plain architecture: the Rio Vero Formation, Spanish Pyrenees. Sedimentary Geology, 139, 229-260.

Jordan, D. W., & Pryor, W. A. (1992). Hierarchical levels of heterogeneity in a Mississippi River meander belt and application to reservoir systems. AAPG Bulletin, 76, 1601-1624.

Keighley, D., Flint, S., Howell, J., & Moscariello, A. (2003). Sequence stratigraphy in lacustrine basins: a model for part of the Green River Formation (Eocene), southwest Uinta Basin, Utah, USA. Journal of Sedimentary Research, 73, 987-1006.

Keller, E. A., & Melhorn, W. N. (1978). Rhythmic spacing and origin of pools and riffles. Geological Society of America Bulletin, 89, 723-730.

Kelly, S. (2006). Scaling and hierarchy in braided rivers and their deposits: examples and implications for reservoir modelling. In: Sambrook Smith, G. H., Best, J. L., Bristow, C. S., Petts, G. E. (eds.), Braided rivers: process, deposits, ecology and management, Special Publication of the International Association of Sedimentologists, 36, 75-106.

Kerr, D. R., Ye, L. S., Bahar, A., Kelkar, B. M., & Montgomery, S. L. (1999). Glenn Pool field, Oklahoma: a case of improved production from a mature reservoir. AAPG Bulletin, 83(1), 1-18.

Kraus M. J., & Middleton L. T. (1987). Contrasting architecture of two alluvial suites in different structural settings. In: Ethridge, F. G., Flores, R. M., Harvey, M. D. (eds.), Recent developments in fluvial sedimentology, SEPM (Society for Sedimentary Geology) Special Publication, 39, 253-262.

Krinitsky, E. L. (1965). Geological Influences on Bank Erosion along Meanders of the Lower Mississippi River, Potamology Investigation, Report 12-15. U.S. Corps of Engineers, Waterways Experiment Station, Vicksburg, MS. 30 pp.

Labourdette, R. (2011). Stratigraphy and static connectivity of braided fluvial deposits of the lower Escanilla Formation, south central Pyrenees, Spain. AAPG Bulletin, 95, 585-617.

Leeder, M. R. (1973). Fluviatile fining-upwards cycles and the magnitude of palaeochannels. Geological Magazine, 110, 265-276.

Leo C. T. (1997). Exploration in the Gulf of Thailand in deltaic reservoirs, related to the Bongkot Field. In: Fraser, A. J., Matthews, S. J., Murphy, R. W. (eds.) Petroleum geology of southeast Asia, Geological Society, London, Special Publications, 126, 77-87.

Leopold, L. B., & Wolman, M. G. (1960). River meanders. Geological Society of America Bulletin, 71, 769-793.

Limarino, C., Tripaldi, A., Marenssi, S., Net, L., Re, G., & Caselli, A. (2001). Tectonic control on the evolution of the fluvial systems of the Vinchina Formation (Miocene), northwestern Argentina. Journal of South American Earth Sciences, 14, 751-762.

Lynds, R., & Hajek, E. (2006). Conceptual model for predicting mudstone dimensions in sandy braided-river reservoirs. AAPG Bulletin, 90, 1273-1288.

Lu, J., Cook, P. J., Hosseini, S. A., Yang, C., Romanak, K. D., Zhang, T., Freifeld, B. M., Smyth, R. C., Zeng, H., & Hovorka, S. D. (2012). Complex fluid flow revealed by monitoring CO2 injection in a fluvial formation. Journal of Geophysical Research: Solid Earth, 117, B03208.

Mack, G. H., Leeder, M., Perez-Arlucea, M., & Bailey, B. D. (2003). Early Permian silt-bed fluvial sedimentation in the Orogrande basin of the Ancestral Rocky Mountains, New Mexico, USA. Sedimentary Geology, 160, 159-178.

Mackay, D. M., & Cherry, J. A. (1989). Groundwater contamination: pump-and-treat remediation. Environmental Science & Technology, 23, 630-636.

Martinius, A. W., & Nieuwenhuijs, R. A. (1995). Geological description of flow units in channel sandstones in a fluvial reservoir analogue (Loranca Basin, Spain). Petroleum Geoscience, 1, 237-252.

Maynard, J. R., Feldman, H. R., & Alway, R. (2010). From bars to valleys: the sedimentology and seismic geomorphology of fluvial to estuarine incised-valley fills of the Grand Rapids Formation (Lower Cretaceous), Iron River Field, Alberta, Canada. Journal of Sedimentary Research, 80, 611-638.

Maynard, K., & Murray, I. (2003). One million years from the Upper Arang Formation, West Natuna Basin, implications for reservoir distribution and facies variation in fluvial deltaic deposits. Indonesian Petroleum Association, 29th Annual Convention Proceedings, vol. 1, 270-276.

McKie, T. (2011). Architecture and behavior of dryland fluvial reservoirs, Triassic Skagerrak Formation, Central North Sea. In: Davidson, S. K., Leleu, S., North, C. P. (eds.), From river to rock record, SEPM (Society for Sedimentary Geology) Special Publication, 97, 189-214.

Miall, A. D. (1988). Architectural elements and bounding surfaces in fluvial deposits: anatomy of the Kayenta Formation (Lower Jurassic), southwest Colorado. Sedimentary Geology, 55, 233-262.

Miall, A. (1996). The geology of fluvial deposits: sedimentary facies, basin analysis, and petroleum geology. Springer, Berlin. 582 pp.

Miall, A. D. (2002). Architecture and sequence stratigraphy of Pleistocene fluvial systems in the Malay Basin, based on seismic time-slice analysis. AAPG Bulletin, 86, 1201-1216.

Miall, A. D. (2006). Reconstructing the architecture and sequence stratigraphy of the preserved fluvial record as a tool for reservoir development: a reality check. AAPG Bulletin, 90, 989-1002.

Miall, A. D., & Turner-Peterson, C. E. (1989). Variations in fluvial style in the Westwater Canyon Member, Morrison Formation (Jurassic), San Juan Basin, Colorado Plateau. Sedimentary Geology, 63, 21-60.

Musial, G., Labourdette, R., Franco, J., & Reynaud, J. Y. (2013). Modeling of a tide-influenced point-bar heterogeneity distribution and Impacts on steam-assisted gravity drainage production: Example from Steepbank River, McMurray Formation, Canada. In: Hein, F. J., Leckie, D., Larter, S., & Suter, J. R. (eds.) Heavy-oil and oil-sand petroleum systems in Alberta and beyond: AAPG Studies in Geology, 64, 545-564

Nanson, G. C., & Hickin, E. J. (1983). Channel migration and incision on the Beatton River. Journal of Hydraulic Engineering, 109, 327-337.

Nanson, G. C., & Hickin, E. J. (1986). A statistical analysis of bank erosion and channel migration in western Canada. Geological Society of America Bulletin, 97, 497-504.

Olsen, H. (1987). Ancient ephemeral stream deposits: a local terminal fan model from the Bunter Sandstone Formation (L. Triassic) in the Tønder-3,-4 and-5 wells, Denmark. In: Frostick L., Reid I. (eds.), Desert sediments: ancient and modern, Geological Society, London, Special Publications, 35, 69-86.

Olsen, H. (1989). Sandstone-body structures and ephemeral stream processes in the Dinosaur Canyon Member, Moenave Formation (Lower Jurassic), Utah, USA. Sedimentary Geology, 61, 207-221.

Olsen, T. (1995a). Sequence stratigraphy, alluvial architecture and potential reservoir heterogeneities of fluvial deposits: evidence from outcrop studies in Price Canyon, Utah (Upper Cretaceous and Lower Tertiary). In: Steel, R. J., Felt, V. L., Johannessen, E. P., & Mathieu, C. (eds.), Sequence Stratigraphy on the Northwest European Margin, Norwegian Petroleum Society Special Publications, 5, 75-96.

Olsen, T. (1995b). Fluvial and fluvio-lacustrine facies and depositional environments of the Maastrichtian to Paleocene North Horn Formation, Price Canyon, Utah. Mountain Geologist, 32, 27-44.

Opluštil, S., Martínek, K., & Tasáryová, Z. (2005). Facies and architectural analysis of fluvial deposits of the Nýřany Member and the Týnec Formation (Westphalian D–Barruelian) in the Kladno-Rakovník and Pilsen basins. Bulletin of Geosciences, 80, 45-66.

Ori, G. G. (1982). Braided to meandering channel patterns in humid-region alluvial fan deposits, River Reno, Po Plain (northern Italy). Sedimentary Geology, 31, 231-248.

Ori, G. G., & Penney, S. R. (1982). The stratigraphy and sedimentology of the Old Red Sandstone sequence at Dunmore East, County Waterford. Journal of Earth Sciences Royal Dublin Society, 5, 43-59.

Páez, R. H., Lawerence, J. J., & Zhang, M. (2010). Compartmentalization or gravity segregation? Understanding and predicting characteristics of near-critical petroleum fluids. In: Jolley, S. J., Fisher, Q. J., Ainsworth, R. B., Vrolijk, P. J., & Delisle, S. (eds.), Reservoir compartmentalization. Geological Society, London, Special Publications, 347, 43-53.

Pakdeesirote, A., Ackagosol, S., Geena, S., Kitvarayut, N., Lewis, K., Tran, T., Wildman, N., Soodsai, A., & Viriyasittigun, P. (2016). Horizontal well injector/producer pair Platong Field, Pattani Basin, Thailand. AAPG Search and Discovery Article #20354.

Pettijohn, F. J., Potter, P. E., & Siever, R. (1973). Sand and Sandstone. Springer, New York. 618 pp.

Posamentier, H. W. (2001). Lowstand alluvial bypass systems: incised vs. unincised. AAPG Bulletin, 85, 1771-1793.

Pranter, M. J., Ellison, A. I., Cole, R. D., & Patterson, P. E. (2007). Analysis and modeling of intermediate-scale reservoir heterogeneity based on a fluvial point-bar outcrop analog, Williams Fork Formation, Piceance Basin, Colorado. AAPG Bulletin, 91, 1025-1051.

Rasmussen, A. M. S. (2005). Reservoir characterization of a fluvial sandstone: depositional environment and heterogeneities in modeling of the Colton Formation, Utah. M.Sc. Thesis, University of Oslo. 135 pp.

Reijenstein, H. M., Posamentier, H. W., & Bhattacharya, J. P. (2011). Seismic geomorphology and high-resolution seismic stratigraphy of inner-shelf fluvial, estuarine, deltaic, and marine sequences, Gulf of Thailand. AAPG Bulletin, 95, 1959-1990.

Renard, P., & Allard, D. (2013). Connectivity metrics for subsurface flow and transport. Advances in Water Resources, 51, 168-196.

Richardson, J. G., Sangree, J. B., & Sneider, R. M. (1987). Meandering stream reservoirs. Journal of Petroleum Technology, 39, 1501-1502.

Ritzi, R. W. (2000). Behavior of indicator variograms and transition probabilities in relation to the variance in lengths of hydrofacies. Water Resources Research, 36, 3375-3381.

Roberts, E. M. (2007). Facies architecture and depositional environments of the Upper Cretaceous Kaiparowits Formation, southern Utah. Sedimentary Geology, 197, 207-233.

Rygel, M. C., & Gibling, M. R. (2006). Natural geomorphic variability recorded in a high-accommodation setting: fluvial architecture of the Pennsylvanian Joggins Formation of Atlantic Canada. Journal of Sedimentary Research, 76, 1230-1251.

Sánchez-Moya, Y., Sopeña, A, & Ramos, A. (1996). Infill architecture of a nonmarine half-graben Triassic basin (central Spain). Journal of Sedimentary Research, 66, 1122-1136.

Santos, M. G., Almeida, R. P., Godinho, L. P., Marconato, A., & Mountney, N. P. (2014). Distinct styles of fluvial deposition in a Cambrian rift basin. Sedimentology, 61, 881-914.

Schenk, C. J. (1992). Geometry of Fluvial Point-Bar Sandstones and Application to Horizontal Drilling. In: Schmoker J. W., Coalson E. B., Brown C. A. (eds.), Geological studies relevant to horizontal drilling: examples from western North America, Rocky Mountain Association of Geologists, Denver, 61-66.

Sendziak, K. L. (2007). Stratigraphic architecture and avulsion deposits of a low net-sand content fluvial succession: Lower Wasatch Formation, Uinta Basin. M.Sc. Thesis, Colorado School of Mines, Golden. 53 pp.

Shepherd, M. (2009). Meandering fluvial reservoirs. In: Shepherd, M., Oil field production geology. AAPG Memoir 91, 261-272.

Shu, X., Hu, Y., Jin, B., Dong, R., Zhou, H., & Wang, J. (2015, September). Modeling method of point bar internal architecture of meandering river reservoir based on meander migration process inversion algorithm and virtual geo-surfaces automatic fitting technology. Society of Petroleum Engineers paper 175013.

Shurygin, A. M. (1976). The probability of finding deposits and some optimal search grids. Mathematical Geology, 8, 323-330.

Sinclair, A. J. (1975). Some considerations regarding grid orientation and sample spacing. In: Elliott, I. L. (ed.), Geochemical Exploration 1974: Proceedings of the fifth International Geochemical Exploration Symposium. Elsevier, Amsterdam. 133-140.

Smalley, P. C., & Hale, N. A. (1996). Early identification of reservoir compartmentalization by combining a range of conventional and novel data types. SPE Formation Evaluation, 11, 163-170, Society of Petroleum Engineers Paper 30533.

Smalley, P. C., & Muggeridge, A. H. (2010). Reservoir compartmentalization: get it before it gets you. In: Jolley, S. J., Fisher, Q. J., Ainsworth, R. B., Vrolijk, P. J., & Delisle, S. (eds.), Reservoir compartmentalization. Geological Society, London, Special Publications, 347, 25-41.

Smith, R. M. H. (1987). Morphology and depositional history of exhumed Permian point bars in the southwestern Karoo, South Africa. Journal of Sedimentary Research, 57, 19-29.

Sonnenberg, S. A., McKenna, D. J., & McKenna, P. J. (1990). Sorrento field, Denver basin, Colorado. In: Sonnenberg, S. A., Shannon, L. T., Rader, K., von Drehle,W. F., Martin, G. W. (eds.), Morrow sandstones of southeast Colorado and adjacent areas. Rocky Mountain Association of Geologists, Denver. 79-90.

Stephens, M. (1994). Architectural element analysis within the Kayenta Formation (Lower Jurassic) using ground-probing radar and sedimentological profiling, southwestern Colorado. Sedimentary Geology, 90, 179-211.

Stewart, D. J. (1983). Possible Suspended-Load Channel Deposits from the Wealden Group (Lower Cretaceous) of Southern England. In: Collinson J. D., Lewin J. (eds.), Modern and ancient fluvial systems, Special Publication of the International Association of Sedimentologists, 6, 369-384.

Testa, S. M., & Winegardner, D. L. (2000). Restoration of contaminated aquifers: petroleum hydrocarbons and organic compounds, 2nd Edition, CRC Press, Boca Raton, FL. 446 pp.

Thomas, R. G., Smith, D. G., Wood, J. M., Visser, J., Calverley-Range, E. A., & Koster, E. H. (1987). Inclined heterolithic stratification—terminology, description, interpretation and significance. Sedimentary Geology, 53, 123-179.

Toonen, W. H., Kleinhans, M. G., & Cohen, K. M. (2012). Sedimentary architecture of abandoned channel fills. Earth Surface Processes and Landforms, 37, 459-472.

Trendell, A. M., Atchley, S. C., & Nordt, L. C. (2013). Facies analysis of a probable large-fluvial-fan depositional system: the Upper Triassic Chinle Formation at Petrified Forest National Park, Arizona, USA. Journal of Sedimentary Research, 83, 873-895.

van Toorenenburg, K. A., Donselaar, M. E., Noordijk, N. A., & Weltje, G. J. (2016). On the origin of crevasse-splay amalgamation in the Huesca fluvial fan (Ebro Basin, Spain): Implications for connectivity in low net-to-gross fluvial deposits. Sedimentary Geology, 343, 156-164.

Viseras, C., Soria, J. M., Durán, J. J., Pla, S., Garrido, G., García-García, F., & Arribas, A. (2006). A large-mammal site in a meandering fluvial context (Fonelas P-1, Late Pliocene, Guadix Basin, Spain): sedimentological keys for its paleoenvironmental reconstruction. Palaeogeography, Palaeoclimatology, Palaeoecology, 242, 139-168.

Voris, H. K. (2000). Maps of Pleistocene sea levels in Southeast Asia: shorelines, river systems and time durations. Journal of Biogeography, 27, 1153-1167.

Wang, K., Wang, H., Shu, X., Zhou, D., Wang, R., Li, Y., Liu, N., Su, Z., & Ren, B. (2016). Super-large scale horizontal well position optimization method and infilling practice in high water-cut large complex fluvial reservoir based on multidisciplinary innovative techniques. In SPE Annual Technical Conference and Exhibition. Society of Petroleum Engineers paper 181889.

Werren, E. G., Shew, R. D., Adams, E. R., & Stancliffe, R. J. (1990). Meander-belt reservoir geology, mid-dip Tuscaloosa, Little Creek field, Mississippi. In: Barwis, J. H., McPherson, J. G., Studlick, J. R. (eds.), Sandstone petroleum reservoirs, Springer, New York. 85-107.

Willems, C. J., Nick, H. M., Donselaar, M. E., Weltje, G. J., & Bruhn, D. F. (2017). On the connectivity anisotropy in fluvial Hot Sedimentary Aquifers and its influence on geothermal doublet performance. Geothermics, 65, 222-233.

Willis, B. J., & Tang, H. (2010). Three-dimensional connectivity of point-bar deposits. Journal of Sedimentary Research, 80, 440-454.

Wu, S., Yue, D., Liu, J., Shu, Q., Fan, Z., & Li, Y. (2008). Hierarchy modeling of subsurface palaeochannel reservoir architecture. Science in China Series D: Earth Sciences, 51, 126-137.

Yue, D., Wu, S., & Liu, J. (2007). An accurate method for anatomizing architecture of subsurface reservoir in point bar of meandering river. Acta Petrolei Sinica, 28, 99-103. In Chinese.